IMA Journal of Numerical Analysis (2024) **00**, 1–35
https://doi.org/10.1093/imanum/drae093

Discontinuous Galerkin discretization of coupled poroelasticity–elasticity problems

Paola F. Antonietti, Michele Botti and Ilario Mazzieri*
MOX - Dipartimento di Matematica, Politecnico di Milano, P.za L. da Vinci, 32, I-20133 Milano, Italy
*Corresponding author: ilario.mazzieri@polimi.it

[Received on 1 June 2023; revised on 20 November 2024]

This work is concerned with the analysis of a space–time finite element discontinuous Galerkin method on polytopal meshes (XT-PolydG) for the numerical discretization of wave propagation in coupled poroelastic–elastic media. The mathematical model consists of the low-frequency Biot's equations in the poroelastic medium and the elastodynamics equation for the elastic one. To realize the coupling suitable transmission conditions on the interface between the two domains are (weakly) embedded in the formulation. The proposed PolydG discretization in space is coupled with a dG time integration scheme, resulting in a full space–time dG discretization. We present the stability analysis for both semidiscrete and fully discrete formulations, and derive error estimates in suitable energy norms. The method is applied to various numerical test cases to verify the theoretical bounds. Examples of physical interest are also presented to investigate the capability of the proposed method in relevant geophysical scenarios.

Keywords: poroelasticity; multiphysics; space–time discontinuous Galerkin methods; polygonal and polyhedral meshes; stability and convergence analysis.

1. Introduction

The numerical simulation of wave propagation in heterogeneous media is an important aspect of a wide range of scientific problems including acoustic engineering (Triebenbacher *et al.*, 2010), vibro-acoustics (Krishnan *et al.*, 2015), aeronautical engineering (Castagnede *et al.*, 1998), biomedical engineering (Haire & Langton, 1999), computational seismology (Carcione, 2014) and oil and gas exploration (Morency *et al.*, 2011; Zhang *et al.*, 2019). In this framework recent studies have been concerned with the propagation of seismic waves in coupled elastic and poroelastic media. For the region of reservoirs Biot's model of poroelastic wave equations is selected, while for the background region (Biot, 1955) the visco-elastic wave equation is employed, cf. Morency & Tromp (2008). Poroelastic–elastic problems model elastic waves impacting a porous material and consequently propagating through it. The coupling between the elastic and the poroelastic domain is a more general realization of the physically consistent transmission conditions discussed in Vashisth *et al.* (1991); Morency & Tromp (2008); Gregor *et al.* (2021). Indeed, in our case, partial filtration at the interface can be also taken into account. Based on a second-order in-time displacement formulation, in this paper, we present a high-order space–time discontinuous Galerkin method on polytopal grids (XT-PolydG) for the discretization of a coupled poroelastic–elastic problem. The theory developed completes the one presented in Antonietti *et al.* (2020a, 2022b), where coupled poroelastic–acoustic and elastic–acoustic problems were studied, respectively. We remark that the geometric flexibility, due to mild regularity requirements on the underlying polytopal mesh, together with the arbitrary-order accuracy featured by the proposed XT-PolydG method is fundamental within the applicative context under investigation as it guarantees the following: (i) *flexibility* in the representation of the geometry; (ii) high level of *accuracy* in both space and time dimensions; (iii) *efficiency* for parallel computation. Finally, the coupling conditions between the elastic and the poroelastic domains are naturally incorporated (in a weak sense) in the proposed scheme.

In the literature we can find many works concerning the numerical discretization of coupled poroelastic models. Here, we recall, e.g., the semianalytical solution and the plane wave decomposition method (Lefeuve-Mesgouez *et al.*, 2012; Peng *et al.*, 2021), the Lagrange Multipliers method (Rockafellar, 1993; Flemisch *et al.*, 2006; Ambartsumyan *et al.*, 2018), the finite and boundary element methods (Bermùdez *et al.*, 2003; Ferro & Mansur, 2006; Flemisch *et al.*, 2010), mixed and discontinuous finite elements (Phillips & Wheeler, 2008; Girault *et al.*, 2011; Bause *et al.*, 2017; Anaya *et al.*, 2020), the spectral and pseudo-spectral element method (Morency & Tromp, 2008; Sidler *et al.*, 2010), the finite difference method (Dai *et al.*, 1995; Wenzlau & Müller, 2009; Masson & Pride, 2010; Zhang & Gao, 2014), the ADER scheme (de la Puente *et al.*, 2008; Dupuy *et al.*, 2011; Chiavassa & Lombard, 2013; Ward *et al.*, 2017; Zhang *et al.*, 2019; Zhan *et al.*, 2020), the virtual element method (Bürger *et al.*, 2021) and the references therein. Here, by taking inspiration from Girault *et al.* (2011), we analyse an interior penalty discontinuous Galerkin formulation of the coupled problem, where the interface conditions are naturally taken into account by the penalization terms. The geometrical flexibility and high-order accuracy of the proposed scheme are ensured by the use of polygonal meshes and by the dG discretization in the time dimension. We refer the reader to Delfour *et al.* (1981); Hughes & Hulbert (1988); French (1993); Johnson (1993) for early results on time dG schemes for wave-type equations, to Abedi *et al.* (2006); van der Vegt *et al.* (2006); Dörfler *et al.* (2016) for first-order hyperbolic problems, to Kretzschmar *et al.* (2016); Barucq *et al.* (2018) and to Gopalakrishnan *et al.* (2017); Moiola & Perugia (2018); Perugia *et al.* (2020) for Trefftz and tent-pitching techniques, to Banks *et al.* (2014); Antonietti *et al.* (2018, 2023b) for the second-order wave equation and to Nochetto *et al.* (2018) for a comprehensive review. On the other hand, regarding polytopal dG methods, we refer the reader to Antonietti *et al.* (2009); Bassi *et al.* (2012); Antonietti *et al.* (2013); Cangiani *et al.* (2016, 2017a); Congreve & Houston (2019); Cangiani *et al.* (2022) for early results on elliptic and parabolic problems, to Antonietti & Mazzieri (2018); Antonietti *et al.* (2020c) for linear and nonlinear hyperbolic problems and to Antonietti *et al.* (2020a,b, 2022a,b) for coupled wave propagation problems. A dG approximation of the fully coupled thermo-poroelastic problem is presented in Antonietti *et al.* (2023a). Wave propagation in thermo-poroelastic media with dG methods is discussed in Bonetti *et al.* (2023).

In this paper we consider a wave propagation problem in a coupled poroelastic–elastic domain with general filtration conditions at the interface. The displacement-based formulation of the second-order in-time problem is discretized first in space with a PolydG scheme; then it is integrated in time with a dG time stepping scheme. We present the convergence analysis of the semidiscrete and fully discrete formulations of the proposed scheme and demonstrate its performance on relevant geophysical problems.

The remaining part of the paper is structured as follows. In Section 2 we present the coupled poroelastic–elastic differential model for wave propagation in heterogeneous media; we discuss the weak formulation and present the stability analysis in the continuous setting. In Section 3 we introduce the polytopal discontinuous Galerkin space discretization and analyse its stability. The convergence analysis of the aforementioned discretization is discussed in Section 4, while a dG time integration scheme and its algebraic formulation are presented in Section 5. Section 6 contains verification test cases to validate the theoretical error bounds, as well as numerical tests of physical interest. Finally, in Section 7 we draw conclusions and discuss perspectives about future work.

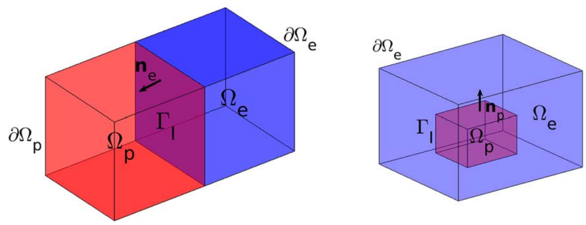

FIG. 1. Simplified representations of the domain $\Omega = \Omega_p \cup \Omega_e$. Here, $\Gamma_I = \partial\Omega_e \cap \partial\Omega_p$ represents the interface between the elastic and the poroelastic domains, where $\partial\Omega_e$ and $\partial\Omega_p$ are the boundaries of elastic and poroelastic sub-domains, respectively.

Notation

Let $\Omega \subset \mathbb{R}^d$, $d = 2, 3$, be an open, convex polygonal/polyhedral domain with Lipschitz boundary $\partial\Omega$. In what follows, for $X \subseteq \Omega$, the notation $\boldsymbol{L}^2(X)$ is adopted in place of $[L^2(X)]^d$, with $d \in \{2, 3\}$. The scalar product in $L^2(X)$ is denoted by $(\cdot,\cdot)_X$, with associated norm $\|\cdot\|_X$. Similarly, $\boldsymbol{H}^\ell(X)$ is defined as $[H^\ell(X)]^d$, with $\ell \geq 0$, equipped with the norm $\|\cdot\|_{\ell,X}$, assuming conventionally that $\boldsymbol{H}^0(X) \equiv \boldsymbol{L}^2(X)$. In addition, we will use $\boldsymbol{H}(\mathrm{div}, X)$ to denote the space of $\boldsymbol{L}^2(X)$ functions with square integrable divergence. For a given final time $T > 0$, $k \in \mathbb{N}$ and a Hilbert space H, the usual notation $C^k([0, T]; H)$ is adopted for the space of H-valued functions, k-times continuously differentiable in $[0, T]$. The notation $x \lesssim y$ stands for $x \leq Cy$, with $C > 0$, independent of the discretization parameters, but possibly dependent on the physical coefficients and the final time T.

2. The physical model and governing equations

The computational domain Ω can be seen as the union of two disjoint, polygonal/polyhedral regions: $\Omega = \Omega_e \cup \Omega_p$, representing the elastic and the poroelastic domains, respectively. The two subdomains share part of their boundary, resulting in the Lipschitz-regular interface $\Gamma_I = \partial\Omega_e \cap \partial\Omega_p$, being $\partial\Omega_e$ and $\partial\Omega_p$ the boundaries of elastic and poroelastic domains, respectively. See Fig. 1. We set $\Gamma_e = \partial\Omega_e \setminus \Gamma_I$ and $\Gamma_p = \partial\Omega_p \setminus \Gamma_I$, so that $\Gamma_i \cap \Gamma_I = \emptyset$ for $i = \{e, p\}$. For the sake of presentation, on Γ_i, $i = \{e, p\}$ we apply homogeneous Dirichlet conditions. The general case follows similarly. Additionally, we suppose that the Hausdorff measures of Γ_e, Γ_p and Γ_I are strictly positive, but the following theory also covers the following cases: (i) $\Omega_p = \Gamma_I = \emptyset$, i.e., $\Omega \equiv \Omega_e$ and (ii) $\Omega_e = \Gamma_I = \emptyset$, i.e., $\Omega \equiv \Omega_p$; as well as (iii) $\partial\Omega_p = \Gamma_I$, i.e., $\Gamma_p = \emptyset$ and (iv) $\partial\Omega_e = \Gamma_I$, i.e., $\Gamma_e = \emptyset$.

The outer unit normal vectors to $\partial\Omega_e$ and $\partial\Omega_p$ are denoted by $\boldsymbol{n}_e$, and $\boldsymbol{n}_p$, respectively, so that $\boldsymbol{n}_p = -\boldsymbol{n}_e$ on Γ_I.

Elastic domain

In the solid elastic domain Ω_e we consider the linear visco-elastodynamics model

$$\rho_e \ddot{\boldsymbol{u}}_e + 2\rho_e\zeta\dot{\boldsymbol{u}}_e + \rho_e\zeta^2\boldsymbol{u}_e - \nabla\cdot\boldsymbol{\sigma}_e(\boldsymbol{u}_e) = \boldsymbol{f}_e, \quad \text{in } \Omega_e \times (0, T], \tag{2.1}$$

where $\boldsymbol{u}_e$ represents the solid displacement, $\rho_e > 0$ is the medium density, $\zeta > 0$ is an attenuation parameter (Antonietti *et al.*, 2022a) and $\boldsymbol{f}_e$ is a given external load. The stress tensor $\boldsymbol{\sigma}_e(\boldsymbol{u})$ is defined as

$$\boldsymbol{\sigma}_e(\boldsymbol{u}) = \mathbb{C} : \boldsymbol{\varepsilon}(\boldsymbol{u}), \tag{2.2}$$

where $\boldsymbol{\varepsilon}(\boldsymbol{u}) = \frac{1}{2}(\nabla\boldsymbol{u} + \nabla\boldsymbol{u}^T)$ is the strain tensor, and $\mathbb{C}$ is the fourth-order, uniformly elliptic elasticity tensor defined by $\mathbb{C} : \boldsymbol{\tau} = 2\mu\boldsymbol{\tau} + \lambda\mathrm{tr}(\boldsymbol{\tau})$ for all $\boldsymbol{\tau} \in \mathbb{R}^{d\times d}$, with $\mathrm{tr}(\boldsymbol{\tau}) = \sum_{i=1}^{d} \boldsymbol{\tau}_{ii}$. Here, $\lambda \geq 0$ and $\mu \geq \mu_0 > 0$ are the Lamé coefficients.

Poroelastic domain

In the poroelastic domain Ω_p, following Antonietti *et al.* (2022b) we consider the low-frequency Biot's equations:

$$\begin{cases} \rho_p\ddot{\boldsymbol{u}}_p + \rho_f\ddot{\boldsymbol{u}}_f + 2\rho_p\zeta\dot{\boldsymbol{u}}_p + \rho_p\zeta^2\boldsymbol{u}_p - \nabla\cdot\boldsymbol{\sigma}_p(\boldsymbol{u}_p,\boldsymbol{u}_f) = \boldsymbol{f}_p, & \text{in } \Omega_p \times (0,T], \\ \rho_f\ddot{\boldsymbol{u}}_p + \rho_w\ddot{\boldsymbol{u}}_f + \frac{\eta}{k}\dot{\boldsymbol{u}}_f + \nabla p(\boldsymbol{u}_p,\boldsymbol{u}_f) = \boldsymbol{g}_p, & \text{in } \Omega_p \times (0,T]. \end{cases} \tag{2.3}$$

Here, $\boldsymbol{u}_p$ and $\boldsymbol{u}_f$ represent the solid and filtration displacements, respectively. In (2.3), the average density ρ_p is given by $\rho_p = \phi\rho_f + (1-\phi)\rho_s$, where $\rho_s > 0$ is the solid density, $\rho_f > 0$ is the saturating fluid density, ρ_w is defined as $\rho_w = \frac{a}{\phi}\rho_f$, being ϕ the *porosity* satisfying $0 < \phi_0 \leq \phi \leq \phi_1 < 1$, and being $a > 1$ the *tortuosity* measuring the deviation of the fluid paths from straight streamlines, cf. Souzanchi *et al.* (2013). The dynamic *viscosity* of the fluid is represented by $\eta > 0$, while the absolute *permeability* by $k > 0$. In (2.3), $\boldsymbol{f}_p$ and $\boldsymbol{g}_p$ are given (regular enough) loading and source terms, respectively. In Ω_p we assume the following constitutive laws, cf. Ezziani (2005), for the stress $\boldsymbol{\sigma}_p$ and pressure p:

$$\boldsymbol{\sigma}_p(\boldsymbol{u}_p,\boldsymbol{u}_f) = \boldsymbol{\sigma}_e(\boldsymbol{u}_p) - \beta\, p(\boldsymbol{u}_p,\boldsymbol{u}_f)\boldsymbol{I}, \qquad p(\boldsymbol{u}_p,\boldsymbol{u}_f) = -m(\beta\nabla\cdot\boldsymbol{u}_p + \nabla\cdot\boldsymbol{u}_f), \tag{2.4}$$

where the Biot–Willis coefficient β and the Biot modulus m are such that $\phi < \beta \leq 1$ and $m \geq m_0 > 0$. A summary of all the model coefficients together with their physical meaning and unit of measure is given in Table 3. To be consistent, in (2.3) we consider the same viscous model as in (2.1). We remark that other viscous models can be considered, see e.g., Morency & Tromp (2008), but are beyond the scope of this work.

Poroelastic–elastic coupling

On Γ_I the coupling between the elastic and the poroelastic domains is achieved by imposing the following transmission conditions, expressing continuity of the normal stresses, the continuity of displacements and the absence of fluid flow into the elastic domain:

$$\boldsymbol{\sigma}_e(\boldsymbol{u}_e)\boldsymbol{n}_e = \boldsymbol{\sigma}_e(\boldsymbol{u}_p)\boldsymbol{n}_p - \delta\beta\, p(\boldsymbol{u}_p,\boldsymbol{u}_f)\boldsymbol{I}\boldsymbol{n}_p, \qquad \text{in } \Gamma_I \times (0,T], \tag{2.5}$$

$$\boldsymbol{u}_e = \boldsymbol{u}_p, \qquad \text{in } \Gamma_I \times (0,T], \tag{2.6}$$

$$((1-\delta)\beta\boldsymbol{u}_p + \boldsymbol{u}_f)\cdot\boldsymbol{n}_p = 0, \qquad \text{in } \Gamma_I \times (0,T], \tag{2.7}$$

for $\delta \in [0,1]$ representing the fluid entry resistance of the interface. In the case $\delta = 1$ condition (2.7) reduces to $\boldsymbol{u}_f \cdot \boldsymbol{n}_p = 0$, namely, there is no filtration through the interface, whereas if $1-\delta = \phi\beta^{-1} < 1$ then (2.7) imposes that the normal component of the fluid displacement $\boldsymbol{u}_p + \phi^{-1}\boldsymbol{u}_f$ is zero, meaning that the fluid is partially flowing into the interface. This assumption on the coupling conditions is somewhat similar to the one that is considered Antonietti *et al.* (2022b) for the poroelastic–acoustic case. For the latter, the continuity of the pressure at the interface was a function of the parameter $\tau \in [0,1]$ modelling the closing/opening of the pores at the interface.

Coupled problem and weak formulation

The coupled *poroelastic–elastic problem* reads as follows: find the vector-field $\boldsymbol{U} = (\boldsymbol{u}_e, \boldsymbol{u}_p, \boldsymbol{u}_f)$ such that $\boldsymbol{u}_e : \Omega_e \times (0,T] \to \mathbb{R}^3$, $\boldsymbol{u}_p : \Omega_p \times (0,T] \to \mathbb{R}^3$ and $\boldsymbol{u}_f : \Omega_p \times (0,T] \to \mathbb{R}^3$ satisfy (2.1)–(2.3) coupled with (2.5)–(2.7). The system is completed by homogeneous Dirichlet boundary conditions, and suitable initial conditions, e.g., $\boldsymbol{U}(\cdot,0) = \boldsymbol{U}_0 = (\boldsymbol{u}_{0e}, \boldsymbol{u}_{0p}, \boldsymbol{u}_{0f})$ and $\dot{\boldsymbol{U}}(\cdot,0) = \boldsymbol{V}_0 = (\boldsymbol{v}_{0e}, \boldsymbol{v}_{0p}, \boldsymbol{v}_{0f})$. In order to state the weak formulation taking into account the essential boundary and transmission conditions we introduce the subspaces

$$\mathbf{V}^{\#} = \{\boldsymbol{v} \in \boldsymbol{H}^1(\Omega_{\#}) \mid \boldsymbol{v}_{|\Gamma_{\#}} = \boldsymbol{0}\}\ \# = \{e,p\},\ \ \mathbf{W}^p = \{\boldsymbol{z} \in \boldsymbol{H}(\mathrm{div}, \Omega_p) \mid (\boldsymbol{z}\cdot \boldsymbol{n}_p)_{|\Gamma_p} = 0\},$$

$$\mathbf{V} = \{(\boldsymbol{v}_e, \boldsymbol{v}_p, \boldsymbol{v}_f) \in \mathbf{V}^e \times \mathbf{V}^{\mathbf{p}} \times \mathbf{W}^{\mathbf{p}} \mid (\boldsymbol{v}_e - \boldsymbol{v}_p)_{|\Gamma_I} = ((1-\delta)\beta \boldsymbol{v}_p + \boldsymbol{v}_f)_{|\Gamma_I} \cdot \boldsymbol{n}_p = 0\}.$$

We also define the space $\mathbf{V}_{\mathbf{0}} = \boldsymbol{L}^2(\Omega_e) \times \boldsymbol{L}^2(\Omega_p) \times \boldsymbol{L}^2(\Omega_p)$ endowed with the norm

$$\|\boldsymbol{U}\|_0^2 = \|\rho_e^{1/2}\boldsymbol{u}_e\|_{\Omega_e}^2 + \|\rho_u^{1/2}\boldsymbol{u}_p\|_{\Omega_p}^2 + \|(\rho_f\phi)^{1/2}(\boldsymbol{u}_p + \phi^{-1}\boldsymbol{u}_f)\|_{\Omega_p}^2 \quad \forall \boldsymbol{U} \in \mathbf{V}_{\mathbf{0}},$$

where $\rho_u = (1-\phi)\rho_s/2$. The weak formulation of problem (2.1)–(2.7) reads as follows: for any time $t \in (0,T]$, find $\boldsymbol{U}(t) \in \mathbf{V}$ s.t.

$$\mathscr{M}(\ddot{\boldsymbol{U}}(t), \boldsymbol{V}) + \mathscr{D}(\dot{\boldsymbol{U}}(t), \boldsymbol{V}) + \mathscr{A}(\boldsymbol{U}(t), \boldsymbol{V}) = \mathscr{F}(\boldsymbol{V})(t) \quad \forall\, \boldsymbol{V} \in \mathbf{V}, \tag{2.8}$$

with $\boldsymbol{U}(\cdot,0) = \boldsymbol{U}_0 \in \mathbf{V}$ and $\dot{\boldsymbol{U}}(\cdot,0) = \boldsymbol{V}_0 \in \mathbf{V}_{\mathbf{0}}$. In (2.8), for any time instant $t \in (0,T]$, $\mathscr{F}(t) : \mathbf{V} \to \mathbb{R}$ is a linear functional defined as

$$\mathscr{F}(\boldsymbol{V})(t) = (\boldsymbol{f}_e(t), \boldsymbol{v}_e)_{\Omega_e} + (\boldsymbol{f}_p(t), \boldsymbol{v}_p)_{\Omega_p} + (\boldsymbol{g}_p(t), \boldsymbol{v}_f)_{\Omega_p} \quad \forall \boldsymbol{V} = (\boldsymbol{v}_e, \boldsymbol{v}_p, \boldsymbol{v}_f) \in \mathbf{V},$$

while for any $\boldsymbol{U}, \boldsymbol{V} \in \mathbf{V}$ we have set

$$\begin{aligned}
\mathscr{M}(\boldsymbol{U}, \boldsymbol{V}) &= (\rho_e \boldsymbol{u}_e, \boldsymbol{v}_e)_{\Omega_e} + (\rho_p \boldsymbol{u}_p + \rho_f \boldsymbol{u}_f, \boldsymbol{v}_p)_{\Omega_p} + (\rho_f \boldsymbol{u}_p + \rho_w \boldsymbol{u}_f, \boldsymbol{v}_f)_{\Omega_p},\\
\mathscr{D}(\boldsymbol{U}, \boldsymbol{V}) &= (2\rho_e\zeta \boldsymbol{u}_e, \boldsymbol{v}_e)_{\Omega_e} + (2\rho_p\zeta \boldsymbol{u}_p, \boldsymbol{v}_p)_{\Omega_p} + (\eta k^{-1}\boldsymbol{u}_f, \boldsymbol{v}_f)_{\Omega_p},\\
\mathscr{A}(\boldsymbol{U}, \boldsymbol{V}) &= (\boldsymbol{\sigma}_e(\boldsymbol{u}_e), \boldsymbol{\varepsilon}(\boldsymbol{v}_e))_{\Omega_e} + (\rho_e\zeta^2 \boldsymbol{u}_e, \boldsymbol{v}_e)_{\Omega_e} + (\boldsymbol{\sigma}_e(\boldsymbol{u}_p), \boldsymbol{\varepsilon}(\boldsymbol{v}_p))_{\Omega_p}\\
&\quad + (\rho_p\zeta^2 \boldsymbol{u}_p, \boldsymbol{v}_p)_{\Omega_p} + (m\nabla\cdot(\beta\boldsymbol{u}_p + \boldsymbol{u}_f), \nabla\cdot(\beta\boldsymbol{v}_p + \boldsymbol{v}_f))_{\Omega_p}.
\end{aligned} \tag{2.9}$$

We close the section with a technical lemma.

LEMMA 2.1. The bilinear forms $\mathscr{M}$ and $\mathscr{D}$ defined in (2.9) are such that

$$\mathscr{M}(\boldsymbol{U}, \boldsymbol{V}) \lesssim \|\boldsymbol{U}\|_0\|\boldsymbol{V}\|_0, \qquad \mathscr{D}(\boldsymbol{U}, \boldsymbol{V}) \lesssim \|\boldsymbol{U}\|_0\|\boldsymbol{V}\|_0 \qquad \forall \boldsymbol{U}, \boldsymbol{V} \in \mathbf{V}_{\mathbf{0}}, \tag{2.10}$$

$$\mathscr{M}(\boldsymbol{U}, \boldsymbol{U}) \gtrsim \|\boldsymbol{U}\|_0^2, \qquad \mathscr{D}(\boldsymbol{U}, \boldsymbol{U}) \gtrsim \|\boldsymbol{U}\|_0^2 \qquad \forall \boldsymbol{U} \in \mathbf{V}_{\mathbf{0}}. \tag{2.11}$$

Proof. Inequalities (2.10) are readily inferred by applying the Cauchy–Schwarz and triangle inequalities. For the first inequality in (2.11) we use the definition of the density functions ρ_e, ρ_p, ρ_u, ρ_w and we observe that $a > 1$ to prove $\mathscr{M}(\boldsymbol{U},\boldsymbol{U}) \gtrsim \|\boldsymbol{U}\|_0^2$, cf. Antonietti *et al.* (2022a). The last inequality in (2.11) follows by the positivity of the coefficients ζ, η and k. □

3. Semidiscrete formulation and stability analysis

We introduce a *polytopic* mesh $\mathscr{T}_h$ made of general polygons (in 2d) or polyhedra (in 3d) and write $\mathscr{T}_h$ as $\mathscr{T}_h = \mathscr{T}_h^e \cup \mathscr{T}_h^p$, where $\mathscr{T}_h^\# = \{\kappa \in \mathscr{T}_h : \overline{\kappa} \subseteq \overline{\Omega_\#}\}$, with $\# = \{e,p\}$. Implicit in this decomposition is the assumption that the meshes $\mathscr{T}_h^e$ and $\mathscr{T}_h^p$ are aligned with Ω_e and Ω_p, respectively. Polynomial degrees $p_{e,\kappa} \geq 1$ and $p_{p,\kappa} \geq 1$ are associated with each element of $\mathscr{T}_h^e$ and $\mathscr{T}_h^p$. The discrete spaces are introduced as follows: $\mathbf{V}_h^e = [\mathscr{P}_{p_e}(\mathscr{T}_h^e)]^d$ and $\mathbf{V}_h^p = [\mathscr{P}_{p_p}(\mathscr{T}_h^p)]^d$, where $\mathscr{P}_r(\mathscr{T}_h^\#)$ is the space of piecewise polynomials in $\Omega_\#$ of total degree less than or equal to r_κ in any $\kappa \in \mathscr{T}_h^\#$ with $\# = \{e,p\}$.

In the following text we assume that $\mathbb{C}$ and m are element-wise constant and we define $\overline{\mathbb{C}}_\kappa = (|\mathbb{C}^{1/2}|_2^2)_{|\kappa}$ for all $\kappa \in \mathscr{T}_h^e \cup \mathscr{T}_h^p$, and $\overline{m}_\kappa = (m)_{|\kappa}$ for all $\kappa \in \mathscr{T}_h^p$. The symbol $|\cdot|_2$ stands for the ℓ^2-norm on $\mathbb{R}^{n\times n}$, with $n = 3$ if $d = 2$ and $n = 6$ if $d = 3$. To deal with polygonal and polyhedral elements we define an *interface* as the intersection of the $(d-1)$-dimensional faces of any two neighbouring elements of $\mathscr{T}_h$. If $d = 2$ an interface/face is a line segment and the set of all interfaces/faces is denoted by $\mathscr{F}_h$. When $d = 3$ an interface can be a general polygon that we assume could be further decomposed into a set of planar triangles collected in the set $\mathscr{F}_h$. We decompose $\mathscr{F}_h$ as $\mathscr{F}_h = \mathscr{F}_h^I \cup \mathscr{F}_h^e \cup \mathscr{F}_h^p$, where $\mathscr{F}_h^I = \{F \in \mathscr{F}_h : F \subset \partial\kappa^e \cap \partial\kappa^p, \kappa^e \in \mathscr{T}_h^e, \kappa^p \in \mathscr{T}_h^p\}$, and $\mathscr{F}_h^e$ and $\mathscr{F}_h^p$ denote all the faces of $\mathscr{T}_h^e$ and $\mathscr{T}_h^p$, respectively, not laying on Γ_I. Finally, the faces of $\mathscr{T}_h^e$ and $\mathscr{T}_h^p$ can be further written as the union of *internal* (i) and *boundary* (b) faces, respectively, i.e., $\mathscr{F}_h^e = \mathscr{F}_h^{e,i} \cup \mathscr{F}_h^{e,0}$ and $\mathscr{F}_h^p = \mathscr{F}_h^{p,i} \cup \mathscr{F}_h^{p,0}$.

Following Cangiani *et al.* (2017b) we next introduce the main assumption on $\mathscr{T}_h$.

Definition 1. A mesh $\mathscr{T}_h$ is said to be *polytopic-regular* if for any $\kappa \in \mathscr{T}_h$ there exists a set of nonoverlapping d-dimensional simplices contained in κ, denoted by $\{S_\kappa^F\}_{F\subset\partial\kappa}$, such that for any face $F \subset \partial\kappa$ it holds $h_\kappa \lesssim d|S_\kappa^F|\,|F|^{-1}$.

In order to avoid technicalities we assume that $\mathscr{T}_h$ satisfies the following assumption.

Assumption 1. The sequence of meshes $\{\mathscr{T}_h\}_h$ is assumed to be *uniformly* polytopic regular in the sense of Definition 1. Moreover the following *hp*-local bounded variation holds: for any pair of neighbouring elements $\kappa^\pm \in \mathscr{T}_h^\#$ it holds $h_{\kappa^+} \lesssim h_{\kappa^-} \lesssim h_{\kappa^+}$, $p_{\#,\kappa^+} \lesssim p_{\#,\kappa^-} \lesssim p_{\#,\kappa^+}$, with $\# = \{e,p\}$.

As pointed out in Cangiani *et al.* (2017b) these assumptions do not impose any restriction on either the number of faces per element or their measure relative to the diameter of the element they belong to. Under (1) the following *trace-inverse inequality* holds:

$$||v||_{L^2(\partial\kappa)} \lesssim p h_\kappa^{-1/2} ||v||_{L^2(\kappa)} \qquad \forall\,\kappa \in \mathscr{T}_h\ \forall v \in \mathscr{P}_p(\kappa). \tag{3.1}$$

Finally, following Arnold *et al.* (2001), for sufficiently piecewise smooth scalar-, vector- and tensor-valued fields ψ, $\boldsymbol{v}$ and $\boldsymbol{\tau}$, respectively, we define the averages and jumps on each *interior* face

$F \in \mathscr{F}_h^{e,i} \cup \mathscr{F}_h^{p,i} \cup \mathscr{F}_h^I$ shared by the elements $\kappa^\pm \in \mathscr{T}_h$ as follows:

$$[\![\psi]\!] = \psi^+ \boldsymbol{n}^+ + \psi^- \boldsymbol{n}^-, \qquad [\![\boldsymbol{v}]\!] = \boldsymbol{v}^+ \otimes \boldsymbol{n}^+ + \boldsymbol{v}^- \otimes \boldsymbol{n}^-, \qquad [\![\boldsymbol{v}]\!]_{\boldsymbol{n}} = \boldsymbol{v}^+ \cdot \boldsymbol{n}^+ + \boldsymbol{v}^- \cdot \boldsymbol{n}^-,$$

$$\{\psi\} = \frac{\psi^+ + \psi^-}{2}, \qquad \{\boldsymbol{v}\} = \frac{\boldsymbol{v}^+ + \boldsymbol{v}^-}{2}, \qquad \{\boldsymbol{\tau}\} = \frac{\boldsymbol{\tau}^+ + \boldsymbol{\tau}^-}{2},$$

where $\otimes$ is the tensor product in $\mathbb{R}^3$, $\cdot^\pm$ denotes the trace on F taken within $\kappa^\pm$ and $\boldsymbol{n}^\pm$ is the outer normal vector to $\partial\kappa^\pm$. Accordingly, on *boundary* faces $F \in \mathscr{F}_h^{e,0} \cup \mathscr{F}_h^{p,0}$, we set $[\![\psi]\!] = \psi\boldsymbol{n}$, $\{\psi\} = \psi$, $[\![\boldsymbol{v}]\!] = \boldsymbol{v} \otimes \boldsymbol{n}$, $[\![\boldsymbol{v}]\!]_{\boldsymbol{n}} = \boldsymbol{v} \cdot \boldsymbol{n}$, $\{\boldsymbol{v}\} = \boldsymbol{v}$, $\{\boldsymbol{\tau}\} = \boldsymbol{\tau}$.

For later use we also define ∇_h and $\nabla_h \cdot$ to be the broken gradient and divergence operators, respectively, set $\boldsymbol{\varepsilon}_h(\boldsymbol{v}) = \frac{\nabla_h \boldsymbol{v} + \nabla_h \boldsymbol{v}^T}{2}$, $\boldsymbol{\sigma}_{eh}(\boldsymbol{v}) = \mathbb{C} : \boldsymbol{\varepsilon}_h(\boldsymbol{v})$ and use the short-hand notation $(\cdot,\cdot)_{\Omega_\#} = \sum_{\kappa \in \mathscr{T}_h^\#} \int_\kappa \cdot$ and $\langle \cdot,\cdot \rangle_{\mathscr{F}_h^\#} = \sum_{F \in \mathscr{F}_h^\#} \int_F \cdot$ for $\# = \{e, p\}$.

3.1 *Semidiscrete PolydG formulation*

We define the space $\mathbf{V_h} = \mathbf{V_h^e} \times \mathbf{V_h^p} \times \mathbf{V_h^p}$ and for any $t \in (0, T]$ denote by $\boldsymbol{U}_h(t) = (\boldsymbol{u}_e, \boldsymbol{u}_p, \boldsymbol{u}_f)_h(t)$ a generic function in $\mathbf{V_h}$. The semidiscrete PolydG formulation of (2.8) reads as follows: find $\boldsymbol{U}_h \in C^2(0, T; \mathbf{V_h})$ such that

$$\begin{cases} \mathscr{M}(\ddot{\boldsymbol{U}}_h(t), \boldsymbol{V}_h) + \mathscr{D}(\dot{\boldsymbol{U}}_h(t), \boldsymbol{V}_h) + \mathscr{A}_h(\boldsymbol{U}_h(t), \boldsymbol{V}_h) + \mathscr{C}_h(\boldsymbol{U}_h(t), \boldsymbol{V}_h) = \mathscr{F}(\boldsymbol{V}_h)(t), \\ (\boldsymbol{U}_h(0), \dot{\boldsymbol{U}}_h(0)) = (\boldsymbol{U}_{0h}, \boldsymbol{V}_{0h}), \end{cases} \tag{3.2}$$

for any $\boldsymbol{V}_h \in \mathbf{V_h}$, and where as initial conditions $\boldsymbol{U}_{0h}$ and $\boldsymbol{V}_{0h}$ we take suitable projections onto $\mathbf{V_h}$ of the initial data. The bilinear forms $\mathscr{M}$ and $\mathscr{D}$ appearing in (3.2) are defined as in (2.9), while

$$\mathscr{A}_h(\boldsymbol{U}, \boldsymbol{V}) = \mathscr{A}_h^e(\boldsymbol{u}_e, \boldsymbol{v}_e) + \mathscr{A}_h^p(\boldsymbol{u}_p, \boldsymbol{v}_p) + \mathscr{B}_h^p(\beta\boldsymbol{u}_p + \boldsymbol{u}_f, \beta\boldsymbol{v}_p + \boldsymbol{v}_f) \tag{3.3}$$

for all $\boldsymbol{U} = (\boldsymbol{u}_e, \boldsymbol{u}_p, \boldsymbol{u}_f)$ and $\boldsymbol{V} = (\boldsymbol{v}_e, \boldsymbol{v}_p, \boldsymbol{v}_f) \in \mathbf{V_h}$ with

$$\begin{aligned} \mathscr{A}_h^\#(\boldsymbol{u}_\#, \boldsymbol{v}_\#) &= (\boldsymbol{\sigma}_{eh}(\boldsymbol{u}_\#), \boldsymbol{\varepsilon}_h(\boldsymbol{v}_\#))_{\Omega_\#} + (\rho_\# \zeta^2 \boldsymbol{u}_\#, \boldsymbol{v}_\#)_{\Omega_\#} - \langle \{\boldsymbol{\sigma}_{eh}(\boldsymbol{u}_\#)\}, [\![\boldsymbol{v}_\#]\!] \rangle_{\mathscr{F}_h^\#} \\ &\quad - \langle [\![\boldsymbol{u}_\#]\!], \{\boldsymbol{\sigma}_{eh}(\boldsymbol{v}_\#)\} \rangle_{\mathscr{F}_h^\#} + \langle \alpha [\![\boldsymbol{u}_\#]\!], [\![\boldsymbol{v}_\#]\!] \rangle_{\mathscr{F}_h^\#}, \quad \# = \{e, p\}, \\ \mathscr{B}_h^p(\boldsymbol{u}, \boldsymbol{v}) &= (m\nabla_h \cdot \boldsymbol{u}, \nabla_h \cdot \boldsymbol{v})_\Omega - \langle \{m(\nabla_h \cdot \boldsymbol{u})\}, [\![\boldsymbol{v}]\!]_{\boldsymbol{n}} \rangle_{\mathscr{F}_h^p} \\ &\quad - \langle [\![\boldsymbol{u}]\!]_{\boldsymbol{n}}, \{m(\nabla_h \cdot \boldsymbol{v})\} \rangle_{\mathscr{F}_h^p} + \langle \gamma [\![\boldsymbol{u}]\!]_{\boldsymbol{n}}, [\![\boldsymbol{v}]\!]_{\boldsymbol{n}} \rangle_{\mathscr{F}_h^p}, \end{aligned} \tag{3.4}$$

cf. also Antonietti *et al.* (2022b). Here, the stabilization functions $\alpha \in L^\infty(\mathscr{F}_h^\#)$, for $\# = \{e,p\}$ and $\gamma \in L^\infty(\mathscr{F}_h^p)$ are defined s.t.

$$\alpha|_F = \begin{cases} c_1 \max\limits_{\kappa\in\{\kappa^+,\kappa^-\}} \left(\overline{\mathbb{C}}_\kappa\, p_{\#,\kappa}^2 h_\kappa^{-1}\right) & \forall F \in \mathscr{F}_h^{\#,i} \cup \mathscr{F}_h^I,\ F \subseteq \partial\kappa^+ \cap \partial\kappa^-, \\ \overline{\mathbb{C}}_\kappa\, p_{\#,\kappa}^2 h_\kappa^{-1} & \forall F \in \mathscr{F}_h^{\#,b}, \qquad F \subseteq \partial\kappa, \end{cases} \tag{3.5}$$

$$\gamma|_F = \begin{cases} c_2 \max\limits_{\kappa\in\{\kappa^+,\kappa^-\}} \left(\overline{m}_\kappa\, p_{p,\kappa}^2 h_\kappa^{-1}\right) & \forall F \in \mathscr{F}_h^{p,i}, \qquad F \subseteq \partial\kappa^+ \cap \partial\kappa^-, \\ \overline{m}_\kappa\, p_{p,\kappa}^2 h_\kappa^{-1} & \forall F \in \mathscr{F}_h^{p,b} \cup \mathscr{F}_h^I,\ F \subseteq \partial\kappa, \kappa \in \mathscr{T}_h^p, \end{cases} \tag{3.6}$$

with positive constants c_1 and c_2 that have to be properly chosen. The definition of the penalty functions (3.5)–(3.6) is based on (Cangiani *et al.*, 2017b, Lemma 35). Alternative stabilization functions can be defined in the spirit of Agut & Diaz (2013). The analysis of the latter is however beyond the scope of this work. The bilinear form $\mathscr{C}_h(\cdot,\cdot)$ is responsible for the coupling between the elastic and the poroelastic domain and is defined as the sum of five contributions, namely,

$$\begin{aligned}\mathscr{C}_h(\boldsymbol{U},\boldsymbol{V}) = \mathscr{A}_{\Gamma_I}^e(\boldsymbol{u}_e,\boldsymbol{v}_e) + \mathscr{A}_{\Gamma_I}^p(\boldsymbol{u}_p,\boldsymbol{v}_p) + \mathscr{B}_{\Gamma_I}^{pp}(\boldsymbol{u}_p,\boldsymbol{v}_p) + \mathscr{B}_{\Gamma_I}^{pf}(\boldsymbol{u}_p,\boldsymbol{v}_f) \\ + \mathscr{B}_{\Gamma_I}^{fp}(\boldsymbol{u}_f,\boldsymbol{v}_p) + \mathscr{B}_{\Gamma_I}^{ff}(\boldsymbol{u}_f,\boldsymbol{v}_f) + \mathscr{C}_{\Gamma_I}^{ep}(\boldsymbol{u}_e,\boldsymbol{v}_p) + \mathscr{C}_{\Gamma_I}^{pe}(\boldsymbol{u}_p,\boldsymbol{v}_e),\end{aligned}$$

for any $\boldsymbol{U},\boldsymbol{V} \in \mathbf{V_h}$, where

$$\begin{aligned}
\mathscr{A}_{\Gamma_I}^e(\boldsymbol{u}_e,\boldsymbol{v}_e) &= \langle \boldsymbol{\sigma}_{eh}(\boldsymbol{u}_e)\boldsymbol{n}_p, \boldsymbol{v}_e\rangle_{\mathscr{F}_h^I} + \langle \boldsymbol{\sigma}_{eh}(\boldsymbol{v}_e)\boldsymbol{n}_p, \boldsymbol{u}_e\rangle_{\mathscr{F}_h^I} + \langle \alpha\boldsymbol{u}_e, \boldsymbol{v}_e\rangle_{\mathscr{F}_h^I},\\
\mathscr{A}_{\Gamma_I}^p(\boldsymbol{u}_p,\boldsymbol{v}_p) &= \langle \alpha\boldsymbol{u}_p, \boldsymbol{v}_p\rangle_{\mathscr{F}_h^I},\\
\mathscr{B}_{\Gamma_I}^{pp}(\boldsymbol{u}_p,\boldsymbol{v}_p) &= -\langle m\beta\nabla_h\cdot\boldsymbol{u}_p, (1-\delta)\beta\boldsymbol{v}_p\cdot\boldsymbol{n}_p\rangle_{\mathscr{F}_h^I} - \langle m\beta\nabla_h\cdot\boldsymbol{v}_p, (1-\delta)\beta\boldsymbol{u}_p\cdot\boldsymbol{n}_p\rangle_{\mathscr{F}_h^I}\\
&\quad + \langle \gamma(1-\delta)\beta\boldsymbol{u}_p\cdot\boldsymbol{n}_p, (1-\delta)\beta\boldsymbol{v}_p\cdot\boldsymbol{n}_p\rangle_{\mathscr{F}_h^I},\\
\mathscr{B}_{\Gamma_I}^{pf}(\boldsymbol{u}_p,\boldsymbol{v}_f) &= -\langle m\beta\nabla_h\cdot\boldsymbol{u}_p, \boldsymbol{v}_f\cdot\boldsymbol{n}_p\rangle_{\mathscr{F}_h^I} - \langle m\nabla_h\cdot\boldsymbol{v}_f, (1-\delta)\beta\boldsymbol{u}_p\cdot\boldsymbol{n}_p\rangle_{\mathscr{F}_h^I}\\
&\quad + \langle \gamma(1-\delta)\beta\boldsymbol{u}_p\cdot\boldsymbol{n}_p, \boldsymbol{v}_f\cdot\boldsymbol{n}_p\rangle_{\mathscr{F}_h^I},\\
\mathscr{B}_{\Gamma_I}^{fp}(\boldsymbol{u}_f,\boldsymbol{v}_p) &= -\langle m\nabla_h\cdot\boldsymbol{u}_f, (1-\delta)\beta\boldsymbol{v}_p\cdot\boldsymbol{n}_p\rangle_{\mathscr{F}_h^I} - \langle m\beta\nabla_h\cdot\boldsymbol{v}_p, \boldsymbol{u}_f\cdot\boldsymbol{n}_p\rangle_{\mathscr{F}_h^I}\\
&\quad + \langle \gamma\boldsymbol{u}_f\cdot\boldsymbol{n}_p, (1-\delta)\beta\boldsymbol{v}_p\cdot\boldsymbol{n}_p\rangle_{\mathscr{F}_h^I},\\
\mathscr{B}_{\Gamma_I}^{ff}(\boldsymbol{u}_f,\boldsymbol{v}_f) &= -\langle m\nabla_h\cdot\boldsymbol{u}_f, \boldsymbol{v}_f\cdot\boldsymbol{n}_p\rangle_{\mathscr{F}_h^I} - \langle m\nabla_h\cdot\boldsymbol{v}_f, \boldsymbol{u}_f\cdot\boldsymbol{n}_p\rangle_{\mathscr{F}_h^I} + \langle \gamma\boldsymbol{u}_f\cdot\boldsymbol{n}_p, \boldsymbol{v}_f\cdot\boldsymbol{n}_p\rangle_{\mathscr{F}_h^I},\\
\mathscr{C}_{\Gamma_I}^{ep}(\boldsymbol{u}_e,\boldsymbol{v}_p) &= -\langle \boldsymbol{\sigma}_{eh}(\boldsymbol{u}_e)\boldsymbol{n}_p, \boldsymbol{v}_p\rangle_{\mathscr{F}_h^I} - \langle \alpha\boldsymbol{u}_e, \boldsymbol{v}_p\rangle_{\mathscr{F}_h^I},\\
\mathscr{C}_{\Gamma_I}^{pe}(\boldsymbol{u}_p,\boldsymbol{v}_e) &= -\langle \boldsymbol{\sigma}_{eh}(\boldsymbol{v}_e)\boldsymbol{n}_p, \boldsymbol{u}_p\rangle_{\mathscr{F}_h^I} - \langle \alpha\boldsymbol{u}_p, \boldsymbol{v}_e\rangle_{\mathscr{F}_h^I}.
\end{aligned} \tag{3.7}$$

The derivation of the coupling bilinear form $\mathscr{C}_h(\cdot,\cdot)$, starting from the strong formulation of the poroelastic–elastic problem, is detailed in the appendix.

The next proposition is a standard result in the framework of dG discretizations and follows from the definition of the functional space $\boldsymbol{V}$, the expression of $\mathscr{C}_h$ given in (5) below and assuming enough sufficient regularity of the continuous solution.

PROPOSITION 1 (Consistency). Assume that for any time $t \in (0,T]$ the solution to the weak problem (2.8) satisfies $\boldsymbol{U}(t) \in \boldsymbol{V} \cap (\boldsymbol{H}^2(\Omega_e) \times \boldsymbol{H}^2(\Omega_p) \times \boldsymbol{H}^2(\Omega_p))$. Then, for all $\boldsymbol{V}_h \in \mathbf{V_h}$,

$$\mathscr{M}(\ddot{\boldsymbol{U}}(t),\boldsymbol{V}_h) + \mathscr{D}(\dot{\boldsymbol{U}}(t),\boldsymbol{V}_h) + \mathscr{A}_h(\boldsymbol{U}(t),\boldsymbol{V}_h) + \mathscr{C}_h(\boldsymbol{U}(t),\boldsymbol{V}_h) = \mathscr{F}(\boldsymbol{V}_h)(t).$$

REMARK 1. Notice that the coupling conditions (2.5) and (2.6) are imposed (weakly) through the bilinear forms $\mathscr{A}_{\Gamma_I}(\cdot,\cdot)$, $\mathscr{A}^p_{\Gamma_I}(\cdot,\cdot)$, $\mathscr{C}^{ep}_{\Gamma_I}(\cdot,\cdot)$ and $\mathscr{C}^{pe}_{\Gamma_I}(\cdot,\cdot)$, while condition (2.7) is included in the bilinear forms $\mathscr{B}^{pp}_{\Gamma_I}(\cdot,\cdot)$, $\mathscr{B}^{pf}_{\Gamma_I}(\cdot,\cdot)$, $\mathscr{B}^{fp}_{\Gamma_I}(\cdot,\cdot)$ and $\mathscr{B}^{ff}_{\Gamma_I}(\cdot,\cdot)$. The latter couples on the interface the filtration displacement in Ω_p to the elastic displacement in Ω_e, through the elastic displacement in Ω_p.

By fixing a basis for the space $\mathbf{V_h}$ and denoting by $\boldsymbol{U}_h = (\boldsymbol{U}_e,\boldsymbol{U}_p,\boldsymbol{U}_f)^T \in \mathbb{R}^{\mathsf{ndof}}$ the vector of the ndof expansion coefficients in the chosen basis of the unknown $\boldsymbol{U}_h$ the semidiscrete formulation (3.2) can be written equivalently as

$$\begin{bmatrix} M^e_{\rho_e} & 0 & 0 \\ 0 & M^p_{\rho} & M^p_{\rho_f} \\ 0 & M^p_{\rho_f} & M^p_{\rho_w} \end{bmatrix} \begin{bmatrix} \ddot{\boldsymbol{U}}_e \\ \ddot{\boldsymbol{U}}_p \\ \ddot{\boldsymbol{U}}_f \end{bmatrix} + \begin{bmatrix} D^e_{\rho_e} & 0 & 0 \\ 0 & D^p_{\rho} & 0 \\ 0 & 0 & D^f \end{bmatrix} \begin{bmatrix} \dot{\boldsymbol{U}}_e \\ \dot{\boldsymbol{U}}_p \\ \dot{\boldsymbol{U}}_f \end{bmatrix}$$
$$+ \begin{bmatrix} A^e_h + A^e_{\Gamma_I} & C^{pe}_{\Gamma_I} & 0 \\ C^{ep}_{\Gamma_I} & A^p + A^p_{\Gamma_I} + B^p_{\beta^2} + B^{pp}_{\Gamma_I} & B^p_{\beta} + B^{fp}_{\Gamma_I} \\ 0 & B^p_{\beta} + B^{pf}_{\Gamma_I} & B^p + B^{ff}_{\Gamma_I} \end{bmatrix} \begin{bmatrix} \boldsymbol{U}_e \\ \boldsymbol{U}_p \\ \boldsymbol{U}_f \end{bmatrix} = \begin{bmatrix} \boldsymbol{F}^e \\ \boldsymbol{F}^p \\ \boldsymbol{G}^p \end{bmatrix} \tag{3.8}$$

with initial conditions $\boldsymbol{U}_{0h}$ and $\boldsymbol{V}_{0h}$. We remark that $\boldsymbol{F}^e$, $\boldsymbol{F}^p$ and $\boldsymbol{G}^p$ are the vector representations of the linear functional $\mathscr{F}$. To ease the notation we set $\boldsymbol{F}_h = [\boldsymbol{F}^e,\boldsymbol{F}^p,\boldsymbol{G}^p]^T$ and we rewrite system (8) in compact form as

$$M\ddot{\boldsymbol{U}}_h(t) + D\dot{\boldsymbol{U}}_h(t) + (A + C)\boldsymbol{U}_h(t) = \boldsymbol{F}_h(t) \quad \forall t \in (0,T]. \tag{3.9}$$

3.2 *Stability analysis*

To carry out the stability analysis of the semidiscrete problem we introduce the energy norm

$$\|\boldsymbol{U}(t)\|^2_{\mathrm{E}} = \|\dot{\boldsymbol{U}}(t)\|^2_0 + |\boldsymbol{U}(t)|^2_{\mathrm{dG}} + |\boldsymbol{U}(t)|^2_{\Gamma_I} + \int_0^t \mathscr{D}(\dot{\boldsymbol{U}},\dot{\boldsymbol{U}})(s)\,\mathrm{d}s + \mathscr{D}(\boldsymbol{U},\boldsymbol{U})(0), \tag{3.10}$$

for all $\boldsymbol{U} = (\boldsymbol{u}_e, \boldsymbol{u}_p, \boldsymbol{u}_f) \in C^1([0,T];\mathbf{V_h})$, where

$$
\begin{aligned}
|\boldsymbol{U}|^2_{\mathrm{dG}} &= \|\boldsymbol{u}_e(t)\|^2_{\mathrm{dG,e}} + \|\boldsymbol{u}_p(t)\|^2_{\mathrm{dG,p}} + |(\beta\boldsymbol{u}_p + \boldsymbol{u}_f)(t)|^2_{\mathrm{dG,p}},\\
\|\boldsymbol{u}_\#\|^2_{\mathrm{dG},\#} &= \|\mathbb{C}^{1/2} : \boldsymbol{\varepsilon}_h(\boldsymbol{u}_\#)\|^2_{\Omega_\star} + \|\alpha^{1/2}[\![\boldsymbol{u}_\#]\!]\|^2_{\mathscr{F}_h^\#} && \forall \boldsymbol{u}_\# \in \mathbf{V_h^\#},\ \# = \{e,p\},\\
|\boldsymbol{u}_p|^2_{\mathrm{dG,p}} &= \|m^{1/2}\nabla_h \cdot \boldsymbol{u}_p\|^2_{\Omega_p} + \|\gamma^{1/2}[\![\boldsymbol{u}_p]\!]_{\boldsymbol{n}}\|^2_{\mathscr{F}_h^p} && \forall \boldsymbol{u}_p \in \mathbf{V_h^p},
\end{aligned}
$$

and for any $(\boldsymbol{u}_e, \boldsymbol{u}_p, \boldsymbol{u}_f) \in \mathbf{V_h^e} \times \mathbf{V_h^p} \times \mathbf{V_h^p}$ we have

$$
|\boldsymbol{U}|^2_{\Gamma_I} = \|\alpha^{1/2}(\boldsymbol{u}_p - \boldsymbol{u}_e)\|^2_{\mathscr{F}_h^I} + \|\gamma^{1/2}((1-\delta)\beta\boldsymbol{u}_p + \boldsymbol{u}_f)\cdot\boldsymbol{n}_p\|^2_{\mathscr{F}_h^I}.
$$

Finally, for all $t \in [0,T]$ we also introduce the norm

$$
|\!|\!|\boldsymbol{U}(t)|\!|\!|^2_{\mathrm{E}} = \|\dot{\boldsymbol{U}}(t)\|^2_0 + |\!|\!|\boldsymbol{U}(t)|\!|\!|^2_{\mathrm{dG}} + |\boldsymbol{U}(t)|^2_{\Gamma_I} + \int_0^t \mathscr{D}(\dot{\boldsymbol{U}},\dot{\boldsymbol{U}})(s)\,\mathrm{d}s + \mathscr{D}(\boldsymbol{U},\boldsymbol{U})(0),
$$

for any $\boldsymbol{U} = (\boldsymbol{u}_e, \boldsymbol{u}_p, \boldsymbol{u}_f) \in \boldsymbol{H}^2(\mathscr{T}_h^e) \times \boldsymbol{H}^2(\mathscr{T}_h^p) \times \boldsymbol{H}^2(\mathscr{T}_h^p)$, where

$$
\begin{aligned}
|\!|\!|\boldsymbol{U}|\!|\!|^2_{\mathrm{dG}} = |\boldsymbol{U}|^2_{\mathrm{dG}} &+ \|\alpha^{-1/2}\{\mathbb{C} : \boldsymbol{\varepsilon}_h(\boldsymbol{u}_e)\}\|^2_{\mathscr{F}_h^e} + \|\alpha^{-1/2}\{\mathbb{C} : \boldsymbol{\varepsilon}_h(\boldsymbol{u}_p)\}\|^2_{\mathscr{F}_h^p}\\
&+ \|\gamma^{-1/2}\{m\nabla_h \cdot (\beta\boldsymbol{u}_p + \boldsymbol{u}_f)\}\|^2_{\mathscr{F}_h^p}.
\end{aligned}
\tag{3.11}
$$

Before showing the main result of the section we introduce the following fundamental lemmas.

LEMMA 3.1. For any $\boldsymbol{U}, \boldsymbol{V} \in \mathbf{V}_h$ and for large enough parameters c_1, c_2 it holds

$$
\mathscr{A}_h(\boldsymbol{U},\boldsymbol{U}) \gtrsim |\boldsymbol{U}|^2_{\mathrm{dG}}, \qquad \mathscr{A}_h(\boldsymbol{U},\boldsymbol{V}) \lesssim |\boldsymbol{U}|_{\mathrm{dG}}|\boldsymbol{V}|_{\mathrm{dG}}.
$$

Proof. For the proof we use the definition of the bilinear form $\mathscr{A}_h(\cdot,\cdot)$ in (3.3) and combine the results in (Antonietti *et al.*, 2022b, Lemma A.3). □

LEMMA 3.2. For any $(\boldsymbol{u}_e, \boldsymbol{u}_p) \in \mathbf{V_h^e} \times \mathbf{V_h^p}$ and any $\boldsymbol{u}_f \in \mathbf{V_h^p}$ it holds

$$
2|\langle\boldsymbol{\sigma}_{eh}(\boldsymbol{u}_e)\boldsymbol{n}_e, \boldsymbol{u}_p - \boldsymbol{u}_e\rangle_{\mathscr{F}_h^I}| \lesssim \frac{1}{\sqrt{c_1}}\|\boldsymbol{u}_e\|_{\mathrm{dG,e}}\|\alpha^{1/2}(\boldsymbol{u}_p - \boldsymbol{u}_e)\|_{\mathscr{F}_h^I}, \tag{3.12}
$$

$$
\begin{aligned}
&2|\langle m\nabla\cdot(\beta\boldsymbol{u}_p + \boldsymbol{u}_f), ((1-\delta)\beta\boldsymbol{u}_p + \boldsymbol{u}_f)\cdot\boldsymbol{n}_p\rangle_{\mathscr{F}_h^I}|\\
&\qquad \lesssim \frac{1}{\sqrt{c_2}}|(\beta\boldsymbol{u}_p + \boldsymbol{u}_f)(t)|_{\mathrm{dG,p}}\|\gamma^{1/2}((1-\delta)\beta\boldsymbol{u}_p + \boldsymbol{u}_f)\cdot\boldsymbol{n}_p\|_{\mathscr{F}_h^I},
\end{aligned}
\tag{3.13}
$$

where c_1 and c_2 are the two positive constants at our disposal appearing in the definition of the stabilization function given in (3.5)–(3.6).

Proof. The proof hinges on Assumption 1 and the trace inverse inequality (3.1). See also (Antonietti *et al.*, 2022b, Lemma A.2). □

COROLLARY 1. For any $\boldsymbol{U} = (\boldsymbol{u}_e, \boldsymbol{u}_p, \boldsymbol{u}_f) \in \mathbf{V_h}$ and for c_1 and c_2 large enough it holds

$$|\boldsymbol{U}|^2_{\mathrm{dG}} + |\boldsymbol{U}|^2_{\Gamma_I} \lesssim \mathscr{A}_h(\boldsymbol{U},\boldsymbol{U}) + \mathscr{C}_h(\boldsymbol{U},\boldsymbol{U}) \lesssim |\boldsymbol{U}|^2_{\mathrm{dG}} + |\boldsymbol{U}|^2_{\Gamma_I}. \tag{3.14}$$

Proof. The proof follows by noting that

$$\begin{aligned}\mathscr{C}_h(\boldsymbol{U},\boldsymbol{W}) = &- 2\langle \boldsymbol{\sigma}_e(\boldsymbol{u}_e)\boldsymbol{n}_p, \boldsymbol{u}_p - \boldsymbol{u}_e\rangle_{\mathscr{F}_h^I} - 2\langle m\nabla\cdot(\beta\boldsymbol{u}_p + \boldsymbol{u}_f), ((1-\delta)\beta\boldsymbol{u}_p + \boldsymbol{u}_f)\cdot\boldsymbol{n}_p\rangle_{\Gamma_I} \\ &+ \|\alpha^{1/2}(\boldsymbol{u}_p - \boldsymbol{u}_f)\|^2_{\mathscr{F}_h^I} + \|\gamma^{1/2}((1-\delta)\beta\boldsymbol{u}_p + \boldsymbol{u}_f)\cdot\boldsymbol{n}_p\|^2_{\mathscr{F}_h^I},\end{aligned}$$

and using the results in Lemma 3.1 and Lemma 3.2. □

LEMMA 3.3. For any $\boldsymbol{U} \in \boldsymbol{H}^2(\mathscr{T}_h^e) \times \boldsymbol{H}^2(\mathscr{T}_h^p) \times \boldsymbol{H}^2(\mathscr{T}_h^p)$ and any $\boldsymbol{V}_h \in \mathbf{V}_h$ it holds

$$\mathscr{A}_h(\boldsymbol{U},\boldsymbol{V}_h) + \mathscr{C}_h(\boldsymbol{U},\boldsymbol{V}_h) \lesssim (|||\boldsymbol{U}|||_{\mathrm{dG}} + |\boldsymbol{U}|_{\Gamma_I})(|\boldsymbol{V}_h|_{\mathrm{dG}} + |\boldsymbol{V}_h|_{\Gamma_I}). \tag{3.15}$$

Proof. The proof is obtained using classical dG arguments and by noting that

$$\begin{aligned}\mathscr{C}_h(\boldsymbol{U},\boldsymbol{V}_h) = &- \langle \boldsymbol{\sigma}_{eh}(\boldsymbol{u}_e)\boldsymbol{n}_p, \boldsymbol{v}_{ph} - \boldsymbol{v}_{eh}\rangle_{\mathscr{F}_h^I} - \langle \boldsymbol{\sigma}_{eh}(\boldsymbol{v}_{eh})\boldsymbol{n}_p, \boldsymbol{u}_p - \boldsymbol{u}_e\rangle_{\mathscr{F}_h^I} \\ &+ \langle \alpha(\boldsymbol{u}_p - \boldsymbol{u}_e), \boldsymbol{v}_{ph} - \boldsymbol{v}_{eh}\rangle_{\mathscr{F}_h^I} \\ &- \langle m\nabla_h\cdot(\beta\boldsymbol{u}_p + \boldsymbol{u}_f), ((1-\delta)\beta\boldsymbol{v}_{ph} + \boldsymbol{v}_{fh})\cdot\boldsymbol{n}_p\rangle_{\mathscr{F}_h^I} \\ &- \langle m\nabla_h\cdot(\beta\boldsymbol{v}_{ph} + \boldsymbol{v}_{fh}), ((1-\delta)\beta\boldsymbol{u}_p + \boldsymbol{u}_f)\cdot\boldsymbol{n}_p\rangle_{\mathscr{F}_h^I} \\ &+ \langle \gamma((1-\delta)\beta\boldsymbol{u}_p + \boldsymbol{u}_f)\cdot\boldsymbol{n}_p, ((1-\delta)\beta\boldsymbol{v}_{ph} + \boldsymbol{v}_{fh})\cdot\boldsymbol{n}_p\rangle_{\mathscr{F}_h^I}.\end{aligned}$$

See also Antonietti & Mazzieri (2018) and (Antonietti *et al.*, 2022b, Lemma A.3). □

The main stability result is stated in the following theorem.

THEOREM 1 (Stability of the semidiscrete formulation). Let Assumption 1 be satisfied. Assume that the problem's data satisfy $(\boldsymbol{f}_e, \boldsymbol{f}_p, \boldsymbol{g}_p) \in L^2((0,T);\mathbf{V_0})$, $\boldsymbol{U}_0 \in \mathbf{V}$ and $\boldsymbol{V}_0 \in \mathbf{V_0}$. For sufficiently large penalty parameters c_1 and c_2 in (3.5) and (3.6), respectively, let $\boldsymbol{U}_h \in C^2(0,T;\mathbf{V_h})$ be a solution of (3.2) for any $t \in (0,T]$. Then, it holds

$$\begin{aligned}\sup_{0\le t\le T} \|\boldsymbol{U}_h(t)\|^2_{\mathrm{E}} \lesssim \|\boldsymbol{U}_{h0}\|^2_{\mathrm{E}} + \int_0^T \Big(&\|(2\rho_e\zeta)^{-1/2}\boldsymbol{f}_e\|^2_{\Omega_e} + \|(2\rho_e\zeta)^{-1/2}\boldsymbol{f}_p\|^2_{\Omega_p} \\ &+ \|(k/\eta)^{1/2}\boldsymbol{g}_p\|^2_{\Omega_p}\Big)\mathrm{d}s,\end{aligned} \tag{3.16}$$

where the hidden constant depends on the final time T, on the penalization parameters c_1 and c_2 in (3.5)–(3.6) and on the material properties.

Proof. By taking $\boldsymbol{V}_h = \dot{\boldsymbol{U}}_h \in \mathbf{V_h}$ in (3.2) we obtain

$$\frac{1}{2}\frac{\mathrm{d}}{\mathrm{d}t}\Big[\mathscr{M}(\dot{\boldsymbol{U}}_h,\dot{\boldsymbol{U}}_h)+\mathscr{A}_h(\boldsymbol{U}_h,\boldsymbol{U}_h)+\mathscr{C}_h(\boldsymbol{U}_h,\boldsymbol{U}_h)\Big]+\mathscr{D}(\dot{\boldsymbol{U}}_h,\dot{\boldsymbol{U}}_h)=\mathscr{F}(\dot{\boldsymbol{U}}_h).$$

Next, we integrate in time between 0 and t, add on both side $\mathscr{D}(\boldsymbol{U}_0,\boldsymbol{U}_0)\geq 0$ and use (3.14) and (2.10)–(2.11) to obtain

$$\|\boldsymbol{U}_h(t)\|_{\mathrm{E}}^2+\int_0^t \mathscr{D}(\dot{\boldsymbol{U}}_h,\dot{\boldsymbol{U}}_h)(s)\,\mathrm{d}s \lesssim \|\boldsymbol{U}_{h0}\|_{\mathrm{E}}^2+\int_0^t \mathscr{F}(\dot{\boldsymbol{U}}_h)(s)\,\mathrm{d}s,$$

for large enough penalty constants c_1 and c_2. Next, to estimate the last term on the right-hand side we use the Cauchy–Schwarz and Young inequalities. □

4. Semidiscrete error analysis

This section is devoted to the semidiscrete error analysis. We first recall some standard interpolation error estimates written in the context of polytopal discretizations and then present the main results of the section. We introduce the following definition and a further mesh assumption (cf. Cangiani *et al.* (2014, 2017b)) to avoid technicalities in the following proofs.

DEFINITION 2. A *covering* $\mathscr{T}_\S = \{\mathscr{K}\}$ of the polytopic mesh $\mathscr{T}_h$ is a set of regular shaped d-dimensional simplices $\mathscr{K}$, $d = 2, 3$, s.t. $\forall\, \kappa \in \mathscr{T}_h$, $\exists\, \mathscr{K} \in \mathscr{T}_\S$ s.t. $\kappa \subseteq \mathscr{K}$.

ASSUMPTION 2. Any mesh $\mathscr{T}_h$ admits a covering $\mathscr{T}_\S$ in the sense of Definition 2 such that (i) $\max_{\kappa\in\mathscr{T}_h} \mathrm{card}\{\kappa' \in \mathscr{T}_h : \kappa' \cap \mathscr{K} \neq \emptyset,\ \mathscr{K} \in \mathscr{T}_\S \text{ s.t. } \kappa \subset \mathscr{K}\} \lesssim 1$ and (ii) $h_{\mathscr{K}} \lesssim h_\kappa$ for each pair $\kappa \in \mathscr{T}_h$, $\mathscr{K} \in \mathscr{T}_\S$ with $\kappa \subset \mathscr{K}$.

For an open bounded polytopic domain $\Sigma \subset \mathbb{R}^d$ and a generic polytopic mesh $\mathscr{T}_h$ over Σ satisfying Assumption 2, as in Cangiani *et al.* (2014), we can introduce the Stein's extension operator $\tilde{\mathscr{E}}: H^m(\kappa) \to H^m(\mathbb{R}^d)$ (Stein, 1970), for any $\kappa \in \mathscr{T}_h$ and $m \in \mathbb{N}_0$, such that $\tilde{\mathscr{E}}v|_\kappa = v$ and $\|\tilde{\mathscr{E}}v\|_{m,\mathbb{R}^d} \lesssim \|v\|_{m,\kappa}$. The corresponding vector-valued version mapping $\boldsymbol{H}^m(\kappa)$ onto $\boldsymbol{H}^m(\mathbb{R}^d)$ acts component-wise and is denoted in the same way. In what follows, for any $\kappa \in \mathscr{T}_h$, we will denote by $\mathscr{K}_\kappa$ the simplex belonging to $\mathscr{T}_\S$ such that $\kappa \subset \mathscr{K}_\kappa$.

The following lemma provides the interpolation bounds that are instrumental for the derivation of the *a priori* error estimate. We remark that the next result holds when Ω is convex.

LEMMA 4.1. For any $\boldsymbol{U} = (\boldsymbol{u}_e, \boldsymbol{u}_p, \boldsymbol{u}_f) \in C^1([0,T]; \mathbf{V} \cap \boldsymbol{H}^m(\mathscr{T}_h^e) \times \boldsymbol{H}^n(\mathscr{T}_h^p) \times \boldsymbol{H}^\ell(\mathscr{T}_h^p))$ with $m, n, \ell \geq 2$ there exists $\boldsymbol{U}_I = (\boldsymbol{u}_e, \boldsymbol{u}_p, \boldsymbol{u}_f)_I \in C^1([0,T]; \mathbf{V_h})$ such that

$$\begin{aligned}\max_{0\leq t\leq T} |||(\boldsymbol{U}-\boldsymbol{U}_I)(t)|||_{\mathrm{E}}^2 \lesssim &\sum_{\kappa\in\mathscr{T}_h^e} \frac{h_\kappa^{2(s_\kappa-1)}}{p_{e,\kappa}^{2m-3}} \mathscr{N}(\boldsymbol{u}_e)_{m,\mathscr{K}_\kappa}^2 + \sum_{\kappa\in\mathscr{T}_h^p} \frac{h_\kappa^{2(q_\kappa-1)}}{p_{p,\kappa}^{2n-3}} \mathscr{N}(\boldsymbol{u}_p)_{n,\mathscr{K}_\kappa}^2 \\ &+ \sum_{\kappa\in\mathscr{T}_h^p} \frac{h_\kappa^{2(r_\kappa-1)}}{p_{p,\kappa}^{2\ell-3}} \mathscr{N}(\boldsymbol{u}_f)_{\ell,\mathscr{K}_\kappa}^2, \end{aligned} \tag{4.1}$$

where $s_\kappa = \min(m, p_{e,\kappa}+1)$, $q_\kappa = \min(n, p_{p,\kappa}+1)$, $r_\kappa = \min(\ell, p_{p,\kappa}+1)$ and

$$\mathscr{N}(\boldsymbol{u})^2_{m,\mathcal{K}_\kappa} = \max_{0\le t\le T}\Big((1+T)\|\widetilde{\mathscr{E}}\dot{\boldsymbol{u}}(t)\|^2_{m,\mathcal{K}_\kappa} + \|\widetilde{\mathscr{E}}\boldsymbol{u}(t)\|^2_{m,\mathcal{K}_\kappa}\Big).$$

Proof. The first part of the proof readily follows by reasoning as in (Antonietti *et al.*, 2020a, Lemma 5.1), cf. also (Antonietti *et al.*, 2022b, Lemma 4.2). To infer estimate (4.1), we resort to the *hp*-approximation properties stated in (Cangiani *et al.*, 2017b, Lemma 23), implying

$$\|\dot{\boldsymbol{U}} - \dot{\boldsymbol{U}}_I\|_0^2 \lesssim \sum_{\kappa\in\mathscr{T}_h^e} \frac{h_\kappa^{2s_\kappa}}{p_{e,\kappa}^{2m}}\|\widetilde{\mathscr{E}}\dot{\boldsymbol{u}}_e\|^2_{m,\mathcal{K}_\kappa} + \sum_{\kappa\in\mathscr{T}_h^p} \frac{h_\kappa^{2q_\kappa}}{p_{p,\kappa}^{2n}}\|\widetilde{\mathscr{E}}\dot{\boldsymbol{u}}_p\|^2_{n,\mathcal{K}_\kappa} + \sum_{\kappa\in\mathscr{T}_h^p} \frac{h_\kappa^{2r_\kappa}}{p_{p,\kappa}^{2\ell}}\|\widetilde{\mathscr{E}}\dot{\boldsymbol{u}}_f\|^2_{\ell,\mathcal{K}_\kappa}.$$

Then, a similar result hods for the terms $\int_0^t \mathscr{D}(\dot{\boldsymbol{U}}-\dot{\boldsymbol{U}}_I, \dot{\boldsymbol{U}}-\dot{\boldsymbol{U}}_I)(s)\,\mathrm{d}s$ and $\mathscr{D}(\boldsymbol{U}-\boldsymbol{U}_I, \boldsymbol{U}-\boldsymbol{U}_I)(0)$. Finally, we bound the term $|\boldsymbol{U}-\boldsymbol{U}_I|^2_{\Gamma_I}$ by applying the triangle and Cauchy–Schwarz inequalities followed by (Cangiani *et al.*, 2017b, Lemma 33), to infer

$$\begin{aligned}
|\boldsymbol{U}-\boldsymbol{U}_I|^2_{\Gamma_I} &\lesssim \|\alpha^{1/2}(\boldsymbol{u}_e - \boldsymbol{u}_{eI})\|^2_{\mathscr{F}_h^I} + \|\alpha^{1/2}(\boldsymbol{u}_p - \boldsymbol{u}_{pI})\|^2_{\mathscr{F}_h^I} \\
&\quad + \|\gamma^{1/2}(1-\delta)\beta(\boldsymbol{u}_p - \boldsymbol{u}_{pI})\cdot\boldsymbol{n}_p\|^2_{\mathscr{F}_h^I} + \|\gamma^{1/2}(\boldsymbol{u}_f - \boldsymbol{u}_{fI})\cdot\boldsymbol{n}_p\|^2_{\mathscr{F}_h^I} \\
&\lesssim \sum_{\kappa\in\mathscr{T}_h^e} \frac{h_\kappa^{2(s_\kappa-1)}}{p_{e,\kappa}^{2m-3}}\|\widetilde{\mathscr{E}}\boldsymbol{u}_e\|^2_{m,\mathcal{K}_\kappa} + \sum_{\kappa\in\mathscr{T}_h^p} \frac{h_\kappa^{2(q_\kappa-1)}}{p_{p,\kappa}^{2n-3}}\|\widetilde{\mathscr{E}}\boldsymbol{u}_p\|^2_{n,\mathcal{K}_\kappa} \\
&\quad + \sum_{\kappa\in\mathscr{T}_h^p} \frac{h_\kappa^{2(r_\kappa-1)}}{p_{p,\kappa}^{2\ell-3}}\|\widetilde{\mathscr{E}}\boldsymbol{u}_f\|^2_{\ell,\mathcal{K}_\kappa}.
\end{aligned}$$

□

Before presenting the main result of this section we set for any time $t\in(0,T]$

$$\boldsymbol{E}(t) = (\boldsymbol{U}-\boldsymbol{U}_h)(t) = (\boldsymbol{u}_e - \boldsymbol{u}_{eh}, \boldsymbol{u}_p - \boldsymbol{u}_{ph}, \boldsymbol{w}_p - \boldsymbol{w}_{ph})(t),$$

and, assuming that $\boldsymbol{U}$ is sufficiently regular, we use the *consistency* of the semidiscrete formulation stated in Proposition 1 to write the following *error equation*:

$$\mathscr{M}(\ddot{\boldsymbol{E}}, \boldsymbol{V}_h) + \mathscr{D}(\dot{\boldsymbol{E}}, \boldsymbol{V}_h) + \mathscr{A}_h(\boldsymbol{E}, \boldsymbol{V}_h) + \mathscr{C}_h(\boldsymbol{E}, \boldsymbol{V}_h) = 0 \quad \forall\, \boldsymbol{V}_h \in \mathbf{V}_h. \tag{4.2}$$

The proof of the following results is rather standard and follows the principles of consistency, discrete stability and continuity of finite element discretizations.

THEOREM 2 (Semidiscrete error estimates). Let Assumption 1 and Assumption 2 hold. Let the solution $\boldsymbol{U} = (\boldsymbol{u}_e, \boldsymbol{u}_p, \boldsymbol{u}_f)$ of problem (2.8) be such that

$$\boldsymbol{U} \in C^2([0,T]; \boldsymbol{H}^m(\mathscr{T}_h^e) \times \boldsymbol{H}^n(\mathscr{T}_h^p) \times \boldsymbol{H}^\ell(\mathscr{T}_h^p)) \cap C^1([0,T]; \mathbf{V}),$$

with $m, n, \ell \geq 2$ and let $\boldsymbol{U}_h = (\boldsymbol{u}_e, \boldsymbol{u}_p, \boldsymbol{u}_f)_h \in C^2([0,T]; \mathbf{V}_h)$ be the solution of (3.2) with c_1 and c_2 sufficiently large. Then, the discretization error $\boldsymbol{E} = \boldsymbol{U} - \boldsymbol{U}_h$ satisfies

$$\max_{0\leq t\leq T} \|\boldsymbol{E}(t)\|_{\mathrm{E}}^2 \lesssim \sum_{\kappa\in\mathscr{T}_h} \frac{h_\kappa^{2(s_\kappa-1)}}{p_{e,\kappa}^{2m-3}} \mathscr{N}(\boldsymbol{u}_e)^2_{m,\mathscr{K}_\kappa} + \sum_{\kappa\in\mathscr{T}_h^p} \frac{h_\kappa^{2(q_\kappa-1)}}{p_{p,\kappa}^{2n-2}} \mathscr{N}(\boldsymbol{u}_p)^2_{n,\mathscr{K}_\kappa} + \sum_{\kappa\in\mathscr{T}_h^p} \frac{h_\kappa^{2(r_\kappa-1)}}{p_{p,\kappa}^{2\ell-3}} \mathscr{N}(\boldsymbol{u}_f)^2_{\ell,\mathscr{K}_\kappa}, \tag{4.3}$$

with $\mathscr{N}(\boldsymbol{u})^2_{m,\mathscr{K}_\kappa} = \max_{0\leq t\leq T}\left(\|\widetilde{\mathscr{E}}\ddot{\boldsymbol{u}}(t)\|^2_{m,\mathscr{K}_\kappa} + \|\widetilde{\mathscr{E}}\dot{\boldsymbol{u}}(t)\|^2_{m,\mathscr{K}_\kappa} + \|\widetilde{\mathscr{E}}\boldsymbol{u}(t)\|^2_{m,\mathscr{K}_\kappa}\right)$ and hidden constant depending on the final time T and the material properties, but independent of the discretization parameters.

Proof. For any time $t \in (0,T]$ let $\boldsymbol{U}_I(t) = (\boldsymbol{u}_e, \boldsymbol{u}_p, \boldsymbol{u}_f)_I(t) \in \mathbf{V}_h$ be the interpolants defined in Lemma 4.1. We split the error as $\boldsymbol{E}(t) = \boldsymbol{E}_I(t) - \boldsymbol{E}_h(t)$, where

$$\begin{aligned}
\boldsymbol{E}_I(t) &= (\boldsymbol{U} - \boldsymbol{U}_I)(t) = (\boldsymbol{u}_e - \boldsymbol{u}_{eI}, \boldsymbol{u}_p - \boldsymbol{u}_{pI}, \boldsymbol{u}_f - \boldsymbol{u}_{fI})(t),\\
\boldsymbol{E}_h(t) &= (\boldsymbol{U}_h - \boldsymbol{U}_I)(t) = (\boldsymbol{u}_{eh} - \boldsymbol{u}_{eI}, \boldsymbol{u}_{ph} - \boldsymbol{u}_{pI}, \boldsymbol{u}_{fh} - \boldsymbol{u}_{fI})(t).
\end{aligned}$$

From the triangle inequality we have $\|\boldsymbol{E}(t)\|_{\mathrm{E}}^2 \leq \|\boldsymbol{E}_h(t)\|_{\mathrm{E}}^2 + \|\boldsymbol{E}_I(t)\|_{\mathrm{E}}^2$, and Lemma 4.1 can be used to bound the term $\|\boldsymbol{E}_I(t)\|_{\mathrm{E}}$. As for the term $\|\boldsymbol{E}_h(t)\|_{\mathrm{E}}$, by taking $\boldsymbol{V}_h = \dot{\boldsymbol{E}}_h \in \mathbf{V}_h$ as test functions in (4.2) and collecting a first time derivative, we obtain

$$\begin{aligned}
\frac{1}{2}\frac{\mathrm{d}}{\mathrm{d}t}\left(\mathscr{M}(\dot{\boldsymbol{E}}_h, \dot{\boldsymbol{E}}_h) + \mathscr{A}_h(\boldsymbol{E}_h, \boldsymbol{E}_h) + \mathscr{C}_h(\boldsymbol{E}_h, \boldsymbol{E}_h)\right) + \mathscr{D}(\dot{\boldsymbol{E}}_h, \dot{\boldsymbol{E}}_h) &= \mathscr{M}(\ddot{\boldsymbol{E}}_I, \dot{\boldsymbol{E}}_h)\\
+ \mathscr{D}(\dot{\boldsymbol{E}}_I, \dot{\boldsymbol{E}}_h) - \mathscr{A}_h(\dot{\boldsymbol{E}}_I, \boldsymbol{E}_h) - \mathscr{C}_h(\dot{\boldsymbol{E}}_I, \boldsymbol{E}_h) &+ \frac{\mathrm{d}}{\mathrm{d}t}\mathscr{A}_h(\boldsymbol{E}_I, \boldsymbol{E}_h) + \frac{\mathrm{d}}{\mathrm{d}t}\mathscr{C}_h(\boldsymbol{E}_I, \boldsymbol{E}_h),
\end{aligned} \tag{4.4}$$

where we have used Leibniz's rule on the term $\mathscr{A}_h(\boldsymbol{E}_I, \dot{\boldsymbol{E}}_h)$ and $\mathscr{C}_h(\boldsymbol{E}_I, \dot{\boldsymbol{E}}_h)$. Now, reasoning as in the proof of Theorem 1, integrating (4) between 0 and $t \leq T$, and assuming for simplicity that we can set the initial conditions of the semidiscrete problem so that $\dot{\boldsymbol{E}}_h(0) = \boldsymbol{E}_h(0) = \boldsymbol{0}$, we get

$$\begin{aligned}
\|\boldsymbol{E}_h(t)\|_{\mathrm{E}}^2 + \int_0^t \mathscr{D}(\dot{\boldsymbol{E}}_h, \dot{\boldsymbol{E}}_h)(s)\,\mathrm{d}s &\lesssim \mathscr{A}_h(\boldsymbol{E}_I, \boldsymbol{E}_h)(t) + \mathscr{C}_h(\boldsymbol{E}_I, \boldsymbol{E}_h)(t)\\
&+ \int_0^t \left(\mathscr{M}(\ddot{\boldsymbol{E}}_I, \dot{\boldsymbol{E}}_h) - \mathscr{A}_h(\dot{\boldsymbol{E}}_I, \boldsymbol{E}_h) - \mathscr{C}_{\Gamma_I}(\dot{\boldsymbol{E}}_I, \boldsymbol{E}_h) + \mathscr{D}(\dot{\boldsymbol{E}}_I, \dot{\boldsymbol{E}}_h)\right)(s)\,\mathrm{d}s.
\end{aligned}$$

Note also that $\mathscr{D}(\boldsymbol{E}_h, \boldsymbol{E}_h)(0) = 0$ under the assumption that $\boldsymbol{U}_h(0) = \boldsymbol{U}_I(0)$. Then, we apply Cauchy–Schwarz and Young inequality together with (3.15) to get

$$\begin{aligned}
\|\boldsymbol{E}_h(t)\|_{\mathrm{E}}^2 &\lesssim |||\boldsymbol{E}_I|||^2_{\mathrm{dG}} + |\boldsymbol{E}_I|^2_{\Gamma_I} + \int_0^t \mathscr{D}(\dot{\boldsymbol{E}}_I, \dot{\boldsymbol{E}}_I)(s)\,\mathrm{d}s\\
&+ \int_0^t (\|\ddot{\boldsymbol{E}}_I\|_0 + |||\dot{\boldsymbol{E}}_I|||_{\mathrm{dG}} + |\dot{\boldsymbol{E}}_I|_{\Gamma_I})(\|\dot{\boldsymbol{E}}_h\|_0 + \|\boldsymbol{E}_h\|_{\mathrm{dG}} + |\boldsymbol{E}_h|_{\Gamma_I})(s)\,\mathrm{d}s.
\end{aligned}$$

We note that the first three addends can be bounded by $|||\boldsymbol{E}_I(t)|||_{\mathrm{E}}^2$. Finally, we take the maximum over $t \in [0,T]$, employ the Cauchy–Schwarz and Young inequality and observe that $\int_0^T |f(s)|\mathrm{d}s \leq T \max_{t\in[0,T]} |f(t)|$ to infer

$$\max_{0\le t\le T} \|\boldsymbol{E}_h(t)\|_{\mathrm{E}}^2 \lesssim \max_{0\le t\le T} |||\boldsymbol{E}_I(t)|||_{\mathrm{E}}^2 + T^2 \max_{0\le t\le T} (\|\ddot{\boldsymbol{E}}_I\|_0^2 + |||\boldsymbol{E}_I|||_{\mathrm{dG}}^2 + |\boldsymbol{E}_I|_{\Gamma_I}^2)(t)$$

$$\lesssim \max_{0\le t\le T} |||\boldsymbol{E}_I(t)|||_{\mathrm{E}}^2 + T^2 \max_{0\le t\le T} |||\dot{\boldsymbol{E}}_I(t)|||_{\mathrm{E}}^2.$$

We conclude by applying the estimates in Lemma 4.1. □

5. dG time discretization

To integrate in time the second-order differential system in (3.9) we adopt the scheme proposed in Antonietti *et al.* (2023b) for the elastodynamics equations, which consists of applying a time dG method to the first-order system

$$N\dot{\boldsymbol{Z}}_h + K\boldsymbol{Z}_h = \widehat{\boldsymbol{F}}_h, \tag{5.1}$$

where $\boldsymbol{Z}_h = [\boldsymbol{U}_h, \boldsymbol{V}_h]^T$, and N and K are defined as

$$N = \begin{bmatrix} I & 0 \\ 0 & M \end{bmatrix} \quad \text{and} \quad K = \begin{bmatrix} 0 & -I \\ A+C & D \end{bmatrix}.$$

Here, we recall that I is the identity matrix, M and D are the symmetric and positive definite matrices, C is the coupling matrix and A is a symmetric and positive semidefinite matrix, cf. (3.9). We remark that concerning the system introduced in Antonietti *et al.* (2023b) here the first equation of (5.1) has not been multiplied by A (that in this case is positive semidefinite). To discretize in time this system we partition the interval $(0,T]$ into N_T time-slabs $I_n = (t_{n-1}, t_n]$ having length $\Delta t_n = t_n - t_{n-1}$, for $n = 1,\dots,N$ with $t_0 = 0$ and $t_N = T$. Then, we introduce the functional spaces

$$\mathbf{V}_{\Delta t_n}^{r_n} = \{\boldsymbol{Z} : I_n \to \mathbb{R}^{2\mathsf{ndof}} \text{ s.t. } \boldsymbol{Z} \in [\mathscr{P}^{r_n}(I_n)]^{2\mathsf{ndof}}, r_n \geq 1\},$$

and

$$\mathbf{V}_{\Delta t}^{r} = \{\boldsymbol{Z} \in \boldsymbol{L}^2(0,T] \text{ s.t. } \boldsymbol{Z}|_{I_n} = [\boldsymbol{U}, \boldsymbol{V}]^T|_{I_n} \in \mathbf{V}_{\Delta t_n}^{r_n}\ \forall\, n = 1, ..., N_T\}. \tag{5.2}$$

We use the notation $[\cdot]_n$ to denote the jump of $\boldsymbol{Z} \in \mathbf{V}_{\Delta t}^r$ at time instant t_n, i.e., $[\boldsymbol{Z}]_n = \boldsymbol{Z}(t_n^+) - \boldsymbol{Z}(t_n^-)$, for $n \geq 0$. With this notation the time-dG formulation of (5.1) reads as follows: find $\boldsymbol{Z}_{\mathrm{dG}} \in \mathbf{V}_{\Delta t}^r$ such that

$$\mathscr{A}_{\mathrm{T}}(\boldsymbol{Z}_{\mathrm{dG}}, \boldsymbol{W}) = \mathscr{G}(\boldsymbol{W}) \qquad \forall\, \boldsymbol{W} \in \mathbf{V}_{\Delta t}^r, \tag{5.3}$$

where the bilinear form $\mathscr{A}_{\mathrm{T}} : \mathbf{V}_{\Delta t}^r \times \mathbf{V}_{\Delta t}^r \to \mathbb{R}$ is defined by

$$\mathscr{A}_{\mathrm{T}}(\boldsymbol{Z}, \boldsymbol{W}) = \sum_{n=1}^{N_T} (N\dot{\boldsymbol{Z}}, \boldsymbol{W})_{I_n} + (K\boldsymbol{Z}, \boldsymbol{W})_{I_n} + \sum_{n=1}^{N_T-1} N[\boldsymbol{Z}]_n \cdot \boldsymbol{W}(t_n^+) + N\boldsymbol{Z}(0^+) \cdot \boldsymbol{W}(0^+),$$

for all $\boldsymbol{Z}, \boldsymbol{W} \in \mathbf{V}^r_{\Delta t}$. The linear functional $\mathscr{G}: \boldsymbol{L}^2(0,T) \to \mathbb{R}$ is defined as

$$\mathscr{G}(\boldsymbol{W}) = \sum_{n=1}^{N_T} (\widehat{\boldsymbol{F}}_h, \boldsymbol{W})_{I_n} + N\boldsymbol{Z}_0 \cdot \boldsymbol{W}(0^+), \tag{5.4}$$

for any $\boldsymbol{W} \in \mathbf{V}^r_{\Delta t}$, being $\boldsymbol{Z}_0 = [\boldsymbol{U}_{0h}, \boldsymbol{V}_{0h}]^T$. We now state the following result.

THEOREM 3. Problem (5.3) admits a unique solution $\boldsymbol{Z}_{\mathrm{dG}} \in \mathbf{V}^r_{\Delta t}$.

Proof. To prove the uniqueness of the discrete solution of (5.3), due to the linearity of the problem, it is enough to consider the data $\mathscr{G}(\boldsymbol{W}) = 0$ for any $\boldsymbol{W} \in \mathbf{V}^r_{\Delta t}$ and prove that $\boldsymbol{Z}_{\mathrm{dG}} = \boldsymbol{0}$. The existence of the solution follows from linearity and finite dimensionality. We start by setting $\boldsymbol{Z} = [\boldsymbol{U}, \boldsymbol{V}]^T$, and rewrite (5.3) in $I_1 = (t_0, t_1]$ as

$$\begin{cases} (\dot{\boldsymbol{U}}, \widetilde{\boldsymbol{U}})_{I_1} - (\boldsymbol{V}, \widetilde{\boldsymbol{U}})_{I_1} + \boldsymbol{U}(0^+) \cdot \widetilde{\boldsymbol{U}}(0^+) = 0 \\ (M\dot{\boldsymbol{V}}, \widetilde{\boldsymbol{V}})_{I_1} + ((A+C)\boldsymbol{U}, \widetilde{\boldsymbol{V}})_{I_1} + (D\boldsymbol{V}, \widetilde{\boldsymbol{V}})_{I_1} + M\boldsymbol{V}(0^+) \cdot \widetilde{\boldsymbol{V}}(0^+) = 0 \end{cases} \tag{5.5}$$

for any $\boldsymbol{W} = [\widetilde{\boldsymbol{U}}, \widetilde{\boldsymbol{V}}]^T \in \mathbf{V}^r_{\Delta t}$. Now, we choose $\widetilde{\boldsymbol{U}} = A\boldsymbol{U}$ and $\widetilde{\boldsymbol{V}} = \boldsymbol{V}$ in (5.5) and sum the two equations to have

$$\frac{1}{2}\boldsymbol{U}(t_1^-)(A+C)\boldsymbol{U}(t_1^-) + \frac{1}{2}\boldsymbol{U}(t_0^+)(A+C)\boldsymbol{U}(t_0^+) + \frac{1}{2}\boldsymbol{V}(t_1^-)M\boldsymbol{V}(t_1^-) + \frac{1}{2}\boldsymbol{V}(t_0^+)M\boldsymbol{V}(t_0^+) + \|D^{\frac{1}{2}}\boldsymbol{V}\|^2_{I_1} = 0,$$

which in turn implies $\boldsymbol{V}(t_1^-) = \boldsymbol{V}(t_0^+) = \boldsymbol{0}$ and $\boldsymbol{V} = \boldsymbol{0}$ in I_1, since M and D are positive definite matrices. Next, we choose $\widetilde{\boldsymbol{U}} = \boldsymbol{U}$ in the first equation in (5.5) to obtain

$$\frac{1}{2}\boldsymbol{U}(t_1^-)^2 + \frac{1}{2}\boldsymbol{U}(t_0^+)^2 = \boldsymbol{0}, \tag{5.6}$$

from which we get $\boldsymbol{U}(t_1^-) = \boldsymbol{U}(t_0^+) = \boldsymbol{0}$. Finally, using the same equation with $\widetilde{\boldsymbol{U}} = \dot{\boldsymbol{U}}$ we can conclude that $\dot{\boldsymbol{U}} = \boldsymbol{0}$ in I_1, which together with (5.6) yields $\boldsymbol{U} = \boldsymbol{0}$ in I_1. The assertion of Theorem 3 follows by repeating the argument on the next intervals I_n, for $n > 1$. □

Using standard arguments it is possible to prove the following.

LEMMA 5.1. Let $\boldsymbol{Z} \in \boldsymbol{H}^2(0,T)$ be the solution of (5.1). Then, the bilinear form that appears in (5.3) is consistent, namely,

$$\mathscr{A}_{\mathrm{T}}(\boldsymbol{Z}_{\mathrm{dG}} - \boldsymbol{Z}, \boldsymbol{W}) = \boldsymbol{0} \qquad \forall\, \boldsymbol{W} \in \mathbf{V}^r_{\Delta t}. \tag{5.7}$$

For any $\boldsymbol{Z} \in \mathbf{V}^r_{\Delta t}$ we introduce the seminorm

$$|\boldsymbol{Z}|^2_{dG} = \mathscr{A}_{\mathrm{T}}(\boldsymbol{Z}, \widehat{A}\boldsymbol{Z}) = \frac{1}{2}\left(\widehat{K}^{\frac{1}{2}}\boldsymbol{Z}(0^+)\right)^2 + \frac{1}{2}\sum_{n=1}^{N_T-1}\left(\widehat{K}^{\frac{1}{2}}[\boldsymbol{Z}]_n\right)^2 + \frac{1}{2}\left(\widehat{K}^{\frac{1}{2}}\boldsymbol{Z}(T^-)\right)^2 + \sum_{n=1}^{N_T}\|\widehat{D}^{\frac{1}{2}}\boldsymbol{Z}\|^2_{I_n},$$

where

$$\widehat{A} = \begin{bmatrix} A+C & 0 \\ 0 & I \end{bmatrix}, \quad \widehat{K} = \begin{bmatrix} A+C & 0 \\ 0 & M \end{bmatrix}, \quad \text{and} \quad \widehat{D} = \begin{bmatrix} 0 & 0 \\ 0 & D \end{bmatrix}.$$

Before presenting the main result of this section we introduce some preliminary results. The interested reader can find the proof in Schötzau & Schwab (2000).

LEMMA 5.2. Let $I = (-1,1)$ and $u \in L^2(I)$ be continuous at $t = 1$; the projector $\Pi^r u \in \mathscr{P}^r(I)$, $r \in \mathbb{N}_0$, defined by the $r+1$ conditions

$$\Pi^r u(1) = u(1), \qquad (\Pi^r u - u, q)_I = 0 \quad \forall\, q \in \mathscr{P}^{r-1}(I), \tag{5.8}$$

is well-posed. Moreover, let $I = (a,b)$, $\Delta t = b-a$, $r \in \mathbb{N}_0$ and $u \in H^{s_0+1}(I)$ for some $s_0 \in \mathbb{N}_0$. Then,

$$||u - \Pi^r u||^2_{L^2(I)} \lesssim \left(\frac{\Delta t}{2}\right)^{2(s+1)} \frac{1}{r^2} \frac{(r-s)!}{(r+s)!} ||u^{(s+1)}||^2_{L^2(I)}, \tag{5.9}$$

and

$$||\dot{u} - \dot{(\Pi^r u)}||^2_{L^2(I)} \lesssim \left(\frac{\Delta t}{2}\right)^{2s} (r+2) \frac{(r-s)!}{(r+s)!} ||u^{(s+1)}||^2_{L^2(I)}, \tag{5.10}$$

for any integer $0 \le s \le \min(r, s_0)$, where the hidden constant depends on s_0, but it is independent from r and Δt.

Next, we set $\boldsymbol{E} = \boldsymbol{Z} - \boldsymbol{Z}_{\mathrm{dG}} = (\boldsymbol{Z} - \Pi_I^r \boldsymbol{Z}) + (\Pi_I^r \boldsymbol{Z} - \boldsymbol{Z}_{\mathrm{dG}}) = \boldsymbol{E}_I + \boldsymbol{E}_h$ and state the following lemma, which is instrumental for the proof of Theorem 4. For the sake of presentation we postpone the proof in Appendix B.

LEMMA 5.3. Let $\boldsymbol{Z}$ be the solution of problem (5.1) and let $\boldsymbol{Z}_{\mathrm{dG}} \in \mathbf{V}^r_{\Delta t}$ be its finite element approximation. Then, it holds

$$\sum_{n=1}^{N} \|\widehat{A}\boldsymbol{E}_h\|^2_{0,I_n} \lesssim |\boldsymbol{E}_h|^2_{dG} + \sum_{n=1}^{N} \|\boldsymbol{E}_I\|^2_{L^2(I_n)}, \tag{5.11}$$

where the hidden constant depends on the norm of the matrices $\widehat{A}, \widehat{K}$ and $\widehat{D}$ and hence on the space discretization parameters h_e, p_e and h_p, p_p.

We now state the following convergence result.

THEOREM 4. Let $\boldsymbol{Z}_0 \in \mathbb{R}^{2\mathsf{ndof}}$. Let $\boldsymbol{Z}$ be the solution of problem (5.1) and let $\boldsymbol{Z}_{\mathrm{dG}} \in \mathbf{V}^r_{\Delta t}$ be its finite element approximation. If $\boldsymbol{Z}|_{I_n} \in \boldsymbol{H}^{s_n+1}(I_n)$, for any $n = 1, \dots, N_T$ with $s_n \ge 1$, then it holds

$$|\boldsymbol{Z} - \boldsymbol{Z}_{dG}|_{dG} \lesssim \sum_{n=1}^{N_T} \left(\frac{\Delta t}{2}\right)^{\mu_n + \frac{1}{2}} \left((r_n+2)\frac{(r_n-\mu_n)!}{(r_n+\mu_n)!}\right)^{\frac{1}{2}} |\boldsymbol{Z}|_{\boldsymbol{H}^{\mu_n+1}(I_n)}, \tag{5.12}$$

where $\mu_n = \min(r_n, s_n)$, for any $n = 1, \dots, N_T$ and the hidden constant depends on the norm of the matrices $N, K, \widehat{A}, \widehat{K}$ and $\widehat{D}$.

Proof. The proof follows the line of (Antonietti *et al.*, 2023b, Theorem 1). Hence, we have $|\boldsymbol{E}|_{dG} \le |\boldsymbol{E}_I|_{dG} + |\boldsymbol{E}_h|_{dG}$. Employing the properties of the projector (5.8) and estimates (5.9) and (5.10) we can bound $|\boldsymbol{E}_I|_{dG}$ as

$$
\begin{aligned}
|\boldsymbol{E}_I|_{dG}^2 &= \frac{1}{2}\Big(\widehat{K}^{\frac{1}{2}}\boldsymbol{E}_I(0^+)\Big)^2 + \frac{1}{2}\sum_{n=1}^{N_T-1}\Big(\widehat{K}^{\frac{1}{2}}[\boldsymbol{E}_I]_n\Big)^2 + \frac{1}{2}\Big(\widehat{K}^{\frac{1}{2}}\boldsymbol{E}_I(T^-)\Big)^2 + \sum_{n=1}^{N_T}\|\widehat{D}^{\frac{1}{2}}\boldsymbol{E}_I\|_{I_n}^2 \\
&= \sum_{n=1}^{N_T}\|\widehat{D}^{\frac{1}{2}}\boldsymbol{E}_I\|_{I_n}^2 + \frac{1}{2}\sum_{n=1}^{N_T}\Big(-\int_{t_{n-1}}^{t_n}\widetilde{K}^{\frac{1}{2}}\dot{\boldsymbol{E}}_I(s)\mathrm{d}s\Big)^2 \\
&\lesssim \sum_{n=1}^{N_T}\Big(||\boldsymbol{E}_I||_{L^2(I_n)}^2 + \Delta t||\dot{\boldsymbol{E}}_I||_{L^2(I_n)}^2\Big) \\
&\lesssim \sum_{n=1}^{N_T}\left(\frac{\Delta t_n}{2}\right)^{2\mu_n+1}(r_n+2)\frac{(r_n-\mu_n)!}{(r_n+\mu_n)!}|\boldsymbol{Z}|_{\boldsymbol{H}^{\mu_n+1}(I_n)}^2,
\end{aligned}
$$

where $\mu_n = \min(r_n, s_n)$, for any $n = 1, \dots, N_T$. Regarding $|\boldsymbol{E}_h|_{dG}$ we use (5.7) and integration by parts to get

$$
\begin{aligned}
|\boldsymbol{E}_h|_{dG}^2 &= \mathscr{A}_{\mathrm{T}}(\boldsymbol{E}_h, \widehat{A}\boldsymbol{E}_h) = -\mathscr{A}_{\mathrm{T}}(\boldsymbol{E}_I, \widehat{A}\boldsymbol{E}_h) \\
&= -\sum_{n=1}^{N_T}(N\dot{\boldsymbol{E}}_I, \widehat{A}\boldsymbol{E}_h)_{I_n} - \sum_{n=1}^{N_T}(K\boldsymbol{E}_I, \widehat{A}\boldsymbol{E}_h)_{I_n} - \sum_{n=0}^{N_T-1}N[\boldsymbol{E}_I]_n\cdot\widehat{A}\boldsymbol{E}_h(t_n^+) \\
&= \quad \sum_{n=1}^{N_T}(N\boldsymbol{E}_I, \widehat{A}\dot{\boldsymbol{E}}_h)_{I_n} - \sum_{n=1}^{N_T}(K\boldsymbol{E}_I, \widehat{A}\boldsymbol{E}_h)_{I_n} - \sum_{n=1}^{N_T-1}N[\boldsymbol{E}_I]_n\cdot\widehat{A}\boldsymbol{E}_h(t_n^-) - N\boldsymbol{E}_I(T^-)\cdot\widehat{A}\boldsymbol{E}_h(T^-) \\
&= -\sum_{n=1}^{N_T}(K\boldsymbol{E}_I, \widehat{A}\boldsymbol{E}_h)_{I_n},
\end{aligned}
$$

since properties (5.8) hold. Thus, we employ the Cauchy–Schwarz and arithmetic–geometric inequalities to obtain

$$
|\boldsymbol{E}_h|_{dG}^2 \le \sum_{n=1}^{N_T}(K\boldsymbol{E}_I, \widehat{A}\boldsymbol{E}_h)_{I_n} \lesssim \sum_{n=1}^{N_T}\frac{1}{2\varepsilon}||\boldsymbol{E}_I||_{L^2(I_n)}^2 + \frac{\varepsilon}{2}||\widehat{A}\boldsymbol{E}_h||_{L^2(I_n)}^2,
$$

or any $\varepsilon > 0$. Then, using (5.11) and choosing ε small enough we have

$$
|\boldsymbol{E}_h|_{dG}^2 \lesssim \sum_{n=1}^{N_T}\left(\frac{\Delta t_n}{2}\right)^{2\mu_n+2}\frac{1}{r_n^2}\frac{(r_n-\mu_n)!}{(r_n+\mu_n)!}|\boldsymbol{Z}|_{\boldsymbol{H}^{\mu_n+1}(I_n)},
$$

where $\mu_n = \min(r_n, s_n)$, for any $n = 1, \dots, N_T$ and the assertion of Theorem 4 follows. □

5.1 *Algebraic formulation*

In practice to compute the discrete solution to (5.3) we iterate over the time intervals, using as initial conditions for I_{n+1} the trace in t_n of the computed solution in the previous interval I_n. Hence, problem (5.3) written for the generic time interval I_n reduces to the following: find $\boldsymbol{Z}^n_{dG} \in \mathbf{V}^{r_n}_{\Delta t_n}$ such that

$$(N\dot{\boldsymbol{Z}}^n_{\mathrm{dG}}, \boldsymbol{W})_{I_n} + (K\boldsymbol{Z}^n_{\mathrm{dG}}, \boldsymbol{W})_{I_n} + N\boldsymbol{Z}^n_{\mathrm{dG}}(t^+_{n-1}) \cdot \boldsymbol{W}(t^+_{n-1}) = (\widehat{\boldsymbol{F}}_h, \boldsymbol{W})_{I_n} + N\boldsymbol{Z}^{n-1}_{\mathrm{dG}}(t^-_{n-1}) \cdot \boldsymbol{W}(t^+_{n-1}). \quad (5.13)$$

Focusing on the generic interval I_n and fixing a basis for the local finite dimensional space $\mathbf{V}^{r_n}_{\Delta t_n}$ we can rewrite (13) as

$$\boldsymbol{A}^n \boldsymbol{\alpha}^n = \boldsymbol{b}^n, \quad (5.14)$$

where on the interval I_n, $\boldsymbol{\alpha}^n \in \mathbb{R}^{2\mathsf{d}}$ is the solution vector (consisting of the expansion coefficients), $\boldsymbol{b}^n \in \mathbb{R}^{2\mathsf{d}}$ corresponds to the data and $\mathsf{d} = \mathsf{ndof}(r_n + 1)$. The system matrix $\boldsymbol{A}^n \in \mathbb{R}^{2\mathsf{d}\times 2\mathsf{d}}$ has the following structure:

$$\boldsymbol{A}^n = (L_1 + L_3) \otimes N + N_2 \otimes K, \quad n = 1, ..., N_T,$$

where the time matrices L_i, $i = 1, 2, 3$, are defined as follows:

$$L_1^{\ell m} = (\dot{\psi}^m, \psi^\ell)_{I_n}, \quad L_2^{\ell m} = (\psi^m, \psi^\ell)_{I_n}, \quad L_3^{\ell m} = \psi^m(t^+_{n-1})\psi^\ell(t^+_{n-1}),$$

for $m, \ell = 1, ..., r_n + 1$, being ψ^k the generic kth basis function in $\mathscr{P}^{r_n}(I_n)$, for $k = 1, ..., r_n + 1$. As noted in (Southworth *et al.*, 2022, Remark 1) the above scheme is equivalent to an implicit Runge–Kutta (IRK) method with $(r_n + 1)$-stages. As in this case, when the entries of the time matrices L_i, $i = 1, .., 3$, and of the right-hand side are computed through a Gauss–Legendre–Lobatto quadrature formula having $r_n + 1$ points and weights, and the basis functions ψ^ℓ are the characteristic polynomials associated with that points, one obtains the so-called IRK-Lobatto IIIC schemes (see, e.g., (Quarteroni *et al.*, 2007, section 11.8.3)). As a consequence scheme (5.14) is L-stable, algebraically stable and thus B-stable. Moreover, as observed in Jay (2015), it is perfectly suited for stiff problems. To numerically solve system (5.14) we set $\boldsymbol{\alpha}^n = (\boldsymbol{\alpha}^n_u, \boldsymbol{\alpha}^n_v)^\top$, $\boldsymbol{b}^n = (\boldsymbol{b}^n_u, \boldsymbol{b}^n_v)^\top$ and apply a block Gaussian elimination getting

$$\begin{bmatrix} I_n \otimes I & -L_5 \otimes I \\ 0 & M_w \end{bmatrix} \begin{bmatrix} \boldsymbol{\alpha}^n_u \\ \boldsymbol{\alpha}^n_v \end{bmatrix} = \begin{bmatrix} (L_4 \otimes I)\boldsymbol{b}^n_u \\ \boldsymbol{b}^n_v - (L_6 \otimes I)\boldsymbol{b}^n_u \end{bmatrix}, \quad (5.15)$$

with $M_w = (L_1 + L_3) \otimes M + L_2 \otimes D + L_7 \otimes (A + C)$ being I_n is the identity matrix of order $r_n + 1$, $L_4 = (L_1 + L_3)^{-1}$, $L_5 = L_4 L_2$, $L_6 = L_2 L_4$ and $L_7 = L_2 L_4 L_2$. Next, we compute $\boldsymbol{\alpha}^n_v$, by solving the linear system $M_w \boldsymbol{\alpha}^n_v = \boldsymbol{b}^n_v - (L_6 \otimes I)\boldsymbol{b}^n_u$ and then we update $\boldsymbol{\alpha}^n_u$ using the first equation.

6. Numerical results

In this section we present numerical results concerning the verification of our scheme on problems with manufactured solutions and the application of the method to cases of geophysical interest. In all

TABLE 1 *Parameters employed for the test case of Section 6.1*

		Ω_p	Ω_e
Fluid	ρ_f	1	–
	η	1	–
Grain	ρ_s (ρ_e)	1	1
	μ	1	1
	ζ	1	1
Matrix	ϕ	0.5	–
	a	1	–
	k	1	–
	λ	1	2
	m	1	–
	β	1	–

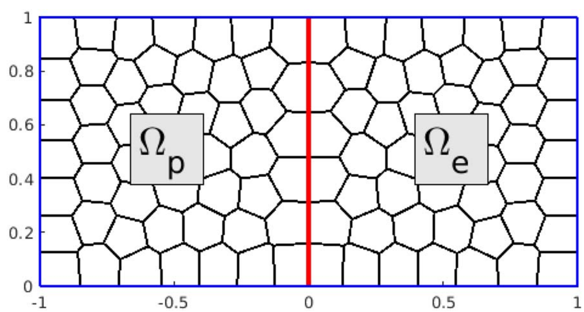

FIG. 2. Test case of Section 6.1. Example of the computational domain having 100 polygonal elements. The red line represents the interface Γ_I.

numerical tests the penalty parameters c_1 and c_2 appearing in definitions (3.5)–(3.6), respectively, have been chosen equal to 10.

6.1 *Verification test*

We consider problem (2.1)–(2.3) coupled with (2.5)–(2.7) in $\Omega = \Omega_e \cup \Omega_p$ with $\Omega_e = (0,1) \times (0,1)$ and $\Omega_p = (-1,0) \times (0,1)$. We choose the exact solution

$$\boldsymbol{u}_e = \cos(\pi\sqrt{2}t)\begin{bmatrix} x^2\sin(2\pi x) \\ x^2\sin(4\pi x)\end{bmatrix}, \quad \boldsymbol{u}_p = \cos(\pi\sqrt{2}t)\begin{bmatrix} x^2\cos(\pi x/2)\sin(\pi x) \\ x^2\cos(\pi x/2)\sin(\pi x)\end{bmatrix}, \tag{6.1}$$

and $\boldsymbol{u}_f = -\boldsymbol{u}_p$. Dirichlet boundary conditions, initial conditions and the forcing term $\boldsymbol{f}_e$,$\boldsymbol{f}_p$ and $\boldsymbol{g}_p$ are set accordingly. For the interface conditions (2.5)–(2.7) we choose $\delta = 1$. The model problem is solved on a sequence of polygonal meshes as the one shown in Fig. 2, with adimensional parameters reported in Table 1.

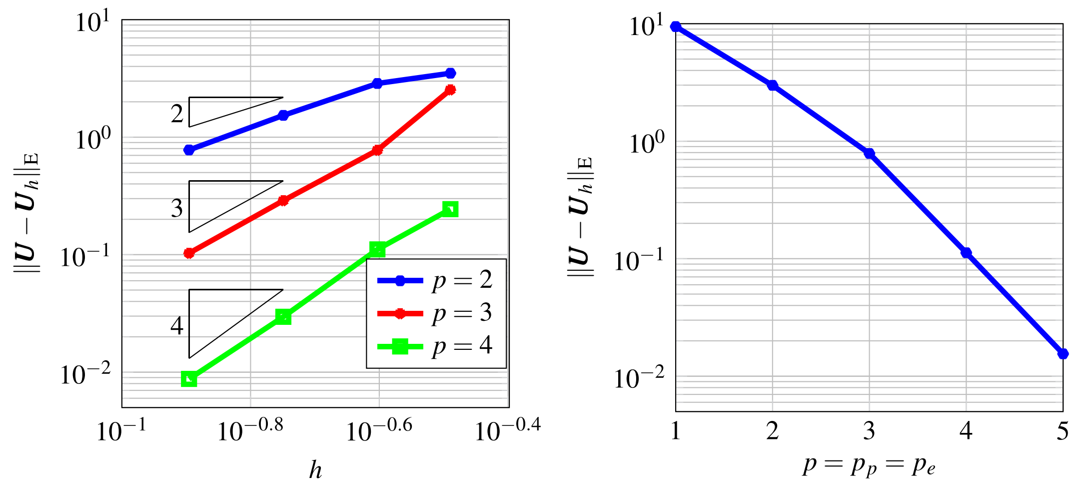

FIG. 3. Test case of Section 6.1. Left: computed energy-errors $\|\boldsymbol{U}-\boldsymbol{U}_{dG}\|_{\mathrm{E}}$ at $T=1$ in logarithmic scale as a function of the mesh size h for different polynomial degrees $p=p_e=p_p$ and fixing the time step $\Delta t=0.001$ and the time polynomial degree $r=1$. The rate of convergence is in agreement with the theoretical estimates in (3). Right: computed energy-errors $\|\boldsymbol{U}-\boldsymbol{U}_{dG}\|_{\mathrm{E}}$ at $T=1$ in semilogarithmic scale as a function of the polynomial degree $p=p_p=p_e$ by fixing the number of elements $N_{el}=100$, the time step $\Delta t=5.e-4$ and the time polynomial degree $r=1$.

As a first test we set the final time equal to 1 and consider, for the time integration scheme in Section 5, a timestep $\Delta t_n=\Delta t=10^{-3}$ and a polynomial degree $r_n=r=1$, for any $n=1,...,1000$. In Fig. 3 (left) we report the computed energy error $\|\boldsymbol{U}-\boldsymbol{U}_h\|_{\mathrm{E}}$ at the final time T, cf. (3.10) as a function of the mesh size h for a polynomial degree $p_e=p_p=2,3,4$. In this case we retrieve the rate of convergence $\mathcal{O}(h^p)$ as proved in (3). In Fig. 3 (right) we report the same results as before as a function of the polynomial degree $p=p_p=p_e$ obtained by fixing the number of grid elements $N_{el}=100$ and considering $\Delta t_n=\Delta t=5.e-4$ and $r_n=r=1$ for $n=1,...,2000$. Notice that this latter case is not covered by our theoretical analysis, nevertheless, we observe numerically optimal convergence.

On the same numerical example we compute numerically the L^2-norm of the error, i.e., $\|\boldsymbol{U}-\boldsymbol{U}_{dG}\|_0$, and the dG-norm of the error, i.e., $|\boldsymbol{Z}-\boldsymbol{Z}_{dG}|_{dG}$, as a function of the time step Δt, by fixing a polygonal mesh of $N_{el}=400$ elements and the polynomial degree $p=p_p=p_e=7$. We compute the error at the final time $T=1$ by choosing different polynomial degrees $r=1,2,3$. As it can be seen from Fig. 4 the estimated order of convergence is $\mathcal{O}(\Delta t^{r+1})$ for the L^2-norm and $\mathcal{O}(\Delta t^{r+\frac{1}{2}})$, for the dG-norm, cf. Theorem 4. Although for the L^2-error this is only numerical evidence, it shows that the considered dG method outperforms classical methods such as the Newmark scheme, which is still widely used for wave propagation problems, see e.g., Antonietti *et al.* (2022b).

Next, in Table 2 we report the computed L^2-error $\|\boldsymbol{U}-\boldsymbol{U}_{dG}\|_0$ as a function of the discretization parameters. In particular, we fix the polynomial degree for both space and time variables and we let N_{el} and Δt vary. It is possible to notice that the spatial discretization error is dominant since we obtain an almost constant value for each row of Table 2. It is interesting to analyse these results in connection with the condition number of the system matrix M_w, cf. Fig. 5 (first row) and the computational time spent for the single run, cf. Fig. 5 (second row). First of all we can observe that the condition number of the system matrix increases by one order whenever the polynomial degree increases by one. Moreover, when fixing the polynomial degree, the matrix M_w is better conditioned for a smaller value of Δt, see Fig. 5 (first row).

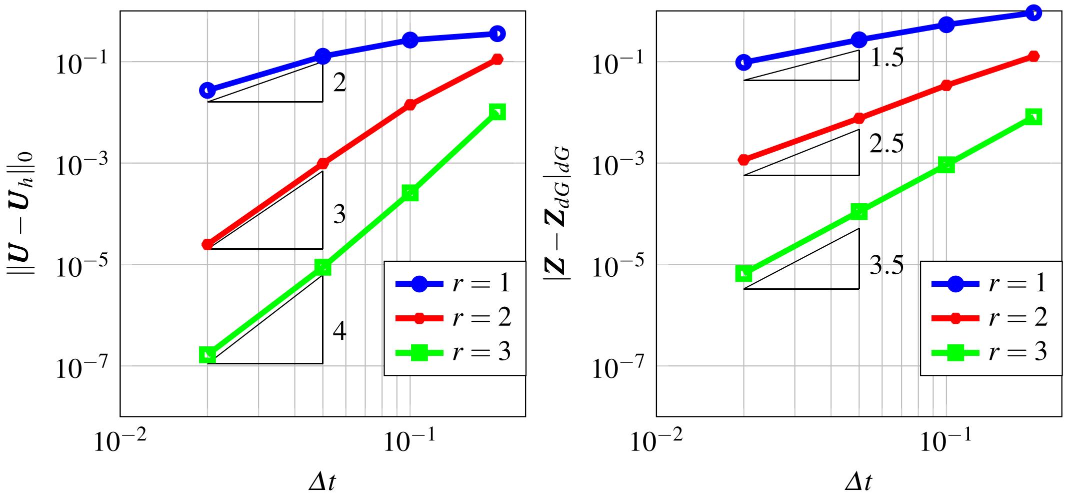

FIG. 4. Test case of Section 6.1. Computed L^2-errors $\|\boldsymbol{U}-\boldsymbol{U}_{dG}\|_0$ (left), and dG-errors $|\boldsymbol{Z}-\boldsymbol{Z}_{dG}|_{dG}$ (right), with $\boldsymbol{Z}=[\boldsymbol{U},\boldsymbol{V}]^T$, at $T=1$ in logarithmic scale as a function of the time step Δt for different polynomial degrees $r=1,2,3$ in time. We set $N_{el}=400$ polygonal elements and a space polynomial degree $p=p_p=p_e=7$.

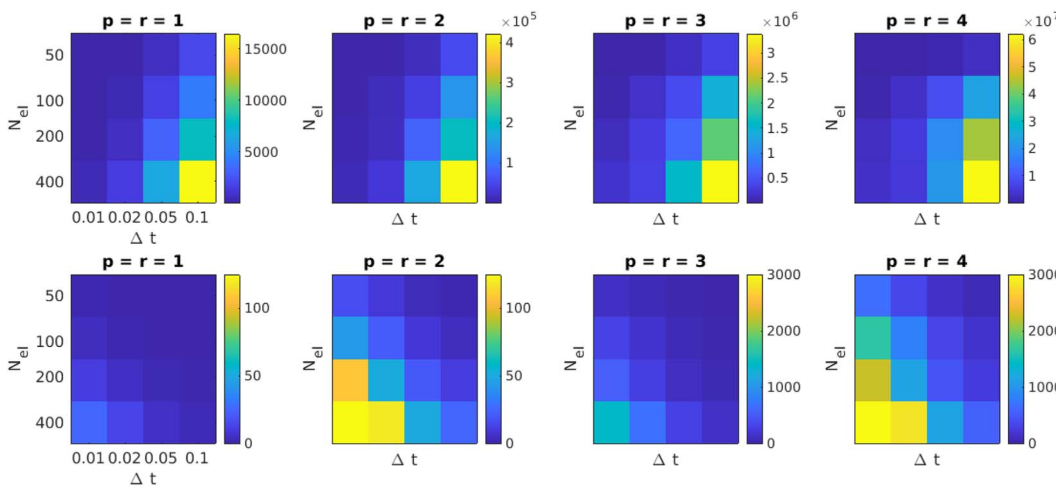

FIG. 5. Test case of Section 6.1. First row: computed condition number (`condest` function in Matlab) as a function of the discretization parameters. Second row: computational time for a single run as a function of the discretization parameters.

Concerning the computational cost, it is obvious that this is proportional to the dimension of the system matrix. Looking at the plot in Fig. 5 (second row) one can observe that even if different combinations of discretization parameters can lead to the same amount of time spent for a single simulation they do not provide the same level of accuracy. Indeed, the sets ($p=r=3, \Delta t=0.01$, $N_{el}=400$) and ($p=r=4, \Delta t=0.02$, $N_{el}=200$) are equivalent from the point of view of the computational cost (1389 s and 1130 s, respectively) but, with the first set we obtain an L^2-error equal to 1.7814e-04, while with the second we get 5.6899e-05.

TABLE 2 *Test case of Section 6.1. Computed L^2-errors $\|\boldsymbol{U} - \boldsymbol{U}_{dG}\|_0$ as a function of the discretization parameters*

	$N_{el} \backslash \Delta t$	0.1	0.05	0.02	0.01
$p = r = 1$	50	2.5734e−01	2.3169e−01	2.1453e−01	2.0908e−01
	100	2.4613e−01	2.0702e−01	1.9284e−01	1.9759e−01
	200	2.4419e−01	1.9706e−01	1.8611e−01	1.8736e−01
	400	2.5188e−01	2.0336e−01	1.7338e−01	1.6802e−01
$p = r = 2$	50	4.8538e−02	4.8105e−02	4.8164e−02	4.8125e−02
	100	5.1387e−02	4.7603e−02	4.7353e−02	4.7406e−02
	200	3.2140e−02	2.7143e−02	2.6818e−02	2.6841e−02
	400	1.5432e−02	8.3925e−03	8.0168e−03	8.0096e−03
$p = r = 3$	50	1.5983e−02	1.5933e−02	1.5947e−02	1.5943e−02
	100	3.1176e−03	3.0956e−03	3.1093e−03	3.1157e−03
	200	8.7709e−04	8.4075e−04	8.4631e−04	8.5067e−04
	400	2.7540e−04	1.7519e−04	1.7682e−04	1.7814e−04
$p = r = 4$	50	9.1399e−04	9.2689e−04	9.3522e−04	9.3748e−04
	100	2.8139e−04	2.8182e−04	2.8601e−04	2.8739e−04
	200	5.6281e−05	5.6095e−05	5.6899e−05	5.7177e−05
	400	1.3301e−05	1.0781e−05	1.0890e−05	1.1072e−05

TABLE 3 *Test case of Section 6.2. Physical parameters for the layered media*

			Proelastic layer	
Fluid	Fluid density	ρ_f	950	kg/m^3
	Dynamic viscosity	η	0 (0.0015)	Pa · s
Grain	Solid density	ρ_s	2200	kg/m^3
	Shear modulus	μ	4.3738×10^9	Pa
Matrix	Porosity	ϕ	0.4	
	Tortuosity	a	2	
	Permeability	k	$1 \cdot 10^{-12}$	m^2
	Lamé coefficient	λ	7.2073×10^9	Pa
	Biot's coefficient	m	6.8386×10^9	Pa
	Biot's coefficient	β	0.0290	
	Damping coefficient	ζ	0 (0.01)	s^{-1}
			Elastic layer	
Matrix	Solid density	ρ	2650	kg/m^3
	Shear modulus	μ	1.5038×10^9	Pa
	Lamé coefficient	λ	1.8121×10^9	Pa
	Damping coefficient	ζ	0 (0.01)	s^{-1}

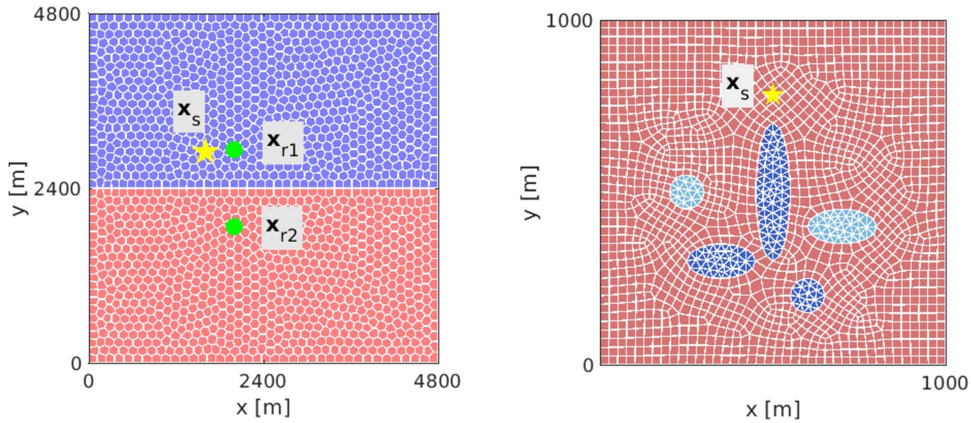

FIG. 6. Left: computational domain for the test case of Section 6.2. Right: computational domain for the test case of Section 6.3. The yellow stars denote the nucleation point $\boldsymbol{x}_s$, while the green dots denote the position of the receivers $\boldsymbol{x}_{r1}$ and $\boldsymbol{x}_{r2}$.

6.2 *Wave propagation in a two-layer medium*

Inspired by Morency & Tromp (2008) we consider a wave propagation problem in a two-layer medium. The computational domain $\Omega = (0, 4800\ m)^2$ and consists of two layers as shown in Fig. 6 (left). We assume the upper layer to be a poroelastic material, while the lower layer to be an elastic medium, cf. Table 3.

An explosive source is located in the upper layer at $\boldsymbol{x}_s = (1600, 2900)\ m$ whose expression is given by

$$\boldsymbol{f}_p = \boldsymbol{g}_p = -M \cdot \nabla\delta(\boldsymbol{x} - \boldsymbol{x}_s)S(t), \tag{6.2}$$

being $M = M_0 I$ the moment tensor with $M_0 > 0$, $\delta(\boldsymbol{x} - \boldsymbol{x}_s)$ is the Dirac delta distribution centred in $\boldsymbol{x}_s$ and $S(t)$ is the source time function. This is a classical choice in the context of earthquake simulation, cf. Morency & Tromp (2008). We consider as a time evolution for $S(t)$ in (6.2) a Ricker-wavelet

$$S(t) = (1 - 2\beta_p(t - t_0)^2)\, e^{-\beta_p(t-t_0)^2}, \quad \beta_p = \pi^2 f_p^2, \tag{6.3}$$

with time-shift $t_0 = 0.3\ s$ and peak-frequency $f_p = 5\ Hz$. Finally, we set $M_0 = 1\ Nm$. We use a shape-regular polygonal mesh with characteristic size $h = 100$ and a polynomial degree $p = 3$ for space discretization. For time integration we set $\Delta t = 0.01$, a polynomial degree $r = 2$ and fix the final time $T = 1.5\ s$. For this model we consider interface conditions (2.5)–(2.7) with $\delta = 1$, free surface boundary conditions on the top boundary, i.e., $\boldsymbol{\sigma}_p \boldsymbol{n}_p = \boldsymbol{0}$, and absorbing boundary conditions on the remaining part of the boundary to avoid artificial reflections and simulate an unbounded medium. In particular, we use the classical first-order paraxial approximations proposed in Stacey (1988) for the elastic boundary Γ_e, i.e.,

$$\boldsymbol{\sigma}_e \boldsymbol{n}_e = \rho(c_p - c_s)(\dot{\boldsymbol{u}}_e \cdot \boldsymbol{n}_e)\boldsymbol{n}_e + \rho_e c_s \dot{\boldsymbol{u}}_e, \tag{6.4}$$

and the ones proposed in Morency & Tromp (2008) for the poroelastic boundary Γ_p, i.e.,

$$\boldsymbol{\sigma}_p\boldsymbol{n}_p = \rho_p c_{pI}(\dot{\boldsymbol{u}}_p\cdot\boldsymbol{n}_p)\boldsymbol{n}_p + \rho_f c_{pII}(\dot{\boldsymbol{u}}_f\cdot\boldsymbol{n}_p)\boldsymbol{n}_p + (\rho_p - \rho_f\phi/a)c_s(I-\boldsymbol{n}_p\boldsymbol{n}_p)\cdot\dot{\boldsymbol{u}}_p,$$
$$-p\boldsymbol{n}_p = \rho_f a/\phi c_{pII}(\dot{\boldsymbol{u}}_f\cdot\boldsymbol{n}_p)\boldsymbol{n}_p + \rho_f c_{pI}(\dot{\boldsymbol{u}}_p\cdot\boldsymbol{n}_p)\boldsymbol{n}_p. \tag{6.5}$$

In (6.4), $c_p = \sqrt{\frac{\lambda+2\mu}{\rho_e}}$ and $c_s = \sqrt{\frac{\mu}{\rho_e}}$ are the compressional and shear wave velocities, respectively, while in (6.5) c_{pI} and c_{pII} are the fast and slow compressional wave velocities, respectively, defined as $c_{pI} = \max\sqrt{\Lambda}$ and $c_{pII} = \min\sqrt{\Lambda}$, where Λ are the solutions of the generalized eigenvalue problem $A\boldsymbol{v} = \Lambda B\boldsymbol{v}$, where

$$A = \begin{bmatrix}\rho_p & \rho_f\\ \rho_f & \rho_w\end{bmatrix}, \quad B = \begin{bmatrix}\lambda+2\mu+m\beta^2 & m\beta\\ m\beta & m\end{bmatrix}.$$

In Fig. 7 we report some snapshots of the vertical component velocity $(\dot{\boldsymbol{u}}_p, \dot{\boldsymbol{u}}_e)_y$ obtained by neglecting or considering viscous effects in the model. In particular, we consider the model TC_1 where $\eta = \zeta = 0$ (Fig. 7, first row) and the model TC_2 with $\eta = 0.0015$ and $\zeta = 0.01$ (Fig. 7, second row). The results of TC_1 are in agreement with the ones presented in Morency & Tromp (2008); Peng *et al.* (2021). From Fig. 7 (first row) we observe the following: (i) the continuity of the velocity field across the interface $\Gamma_I = (0, 4800)\ m \times \{2400\}\ m$; (ii) the propagation of the direct fast c_{pI} compressional wave (first front), the reflected fast c_{pI} compressional wave (second front), the reflected shear c_s (third front) and slow compressional c_{pII} wave (fourth front) in the upper poroelastic layer; (iii) the transmitted compressional c_p and shear c_s wave in the lower elastic layer. The same physical phenomena, although less evident, are present when the viscous damping terms are introduced in TC_2, cf. Fig. 7 (second row). The transmitted shear c_s and the reflected slow longitudinal c_{PII} waves are too weak to be visible at this scale. From the plot we can also see the effect of the first-order absorbing boundaries, which are not perfectly transparent. Recent studies have adopted an efficient perfectly matched layer (PML) methodology, e.g., Martin *et al.* (2008); He *et al.* (2019). The PML implementation is not included in this paper, but will be addressed in the future.

In Fig. 8 we compare the time histories velocities $(\dot{\boldsymbol{u}}_p, \dot{\boldsymbol{u}}_e)$ at the two receivers $\boldsymbol{x}_{r1} = (2000, 2934)\ m$ and at $\boldsymbol{x}_{r2} = (2000, 1867)\ m$ for the different modelling assumptions. Again, here we notice the effect of the damping assumption on the scattered wave field.

6.3 *Wave propagation in an elastic domain with poroelastic inclusions*

To demonstrate the feasibility of tackling a more complex model with the proposed method we consider a coupled elastic–poroelastic model shown in Fig. 6 (right). The background medium is regarded as perfectly elastic (whose mechanical properties are listed in Table 3), while the circle and ellipses with different sizes represent oil and gas reservoirs, which are modelled as poroelastic media. This example takes inspiration from the one proposed in Zhang *et al.* (2019). The poroelastic domains have different material properties: for the domains depicted in light blue in Fig. 6 (right) we consider the values in Table 3, while for the remaining ones we use the ones in Table 4.

We consider a seismic source as in the previous test case applied to the point $\boldsymbol{x}_s = (500, 780)\ m$, with time variation given by a Ricker wavelet with time shift $t_0 = 0.2\ s$ and peak frequency $f_p = 10\ Hz$, cf. (6.3). We consider absorbing boundary conditions for the external elastic domain, cf. (6.4), while we

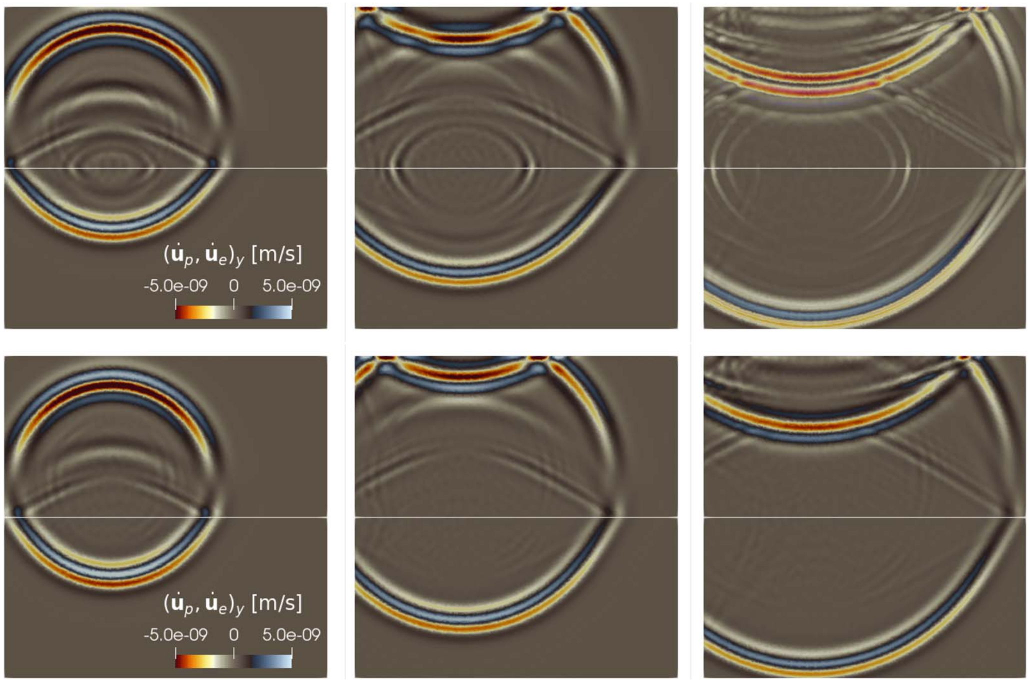

FIG. 7. Test case of Section 6.2. Snapshots of the vertical component velocity $(\dot{\boldsymbol{u}}_p, \dot{\boldsymbol{u}}_e)_y$ at different time instants: $t = 0.9s$ (left), $t = 1.2s$ (centre) and $t = 1.5s$ (right). The top and bottom rows refer to the model TC_1 and TC_2, respectively.

TABLE 4 *Test case of Section 6.3: physical parameters for the dark blue poroelastic domain in Fig. 6 (right)*

			Proelastic layer	
Fluid	Fluid density	ρ_f	750	$\mathrm{kg/m^3}$
	Dynamic viscosity	η	0	$\mathrm{Pa \cdot s}$
Grain	Solid density	ρ_s	2650	$\mathrm{kg/m^3}$
	Shear modulus	μ	1.503×10^9	Pa
Matrix	Porosity	ϕ	0.2	
	Tortuosity	a	2	
	Permeability	k	$1 \cdot 10^{-12}$	$\mathrm{m^2}$
	Lamé coefficient	λ	1.8121×10^9	Pa
	Biot's coefficient	m	7.2642×10^9	Pa
	Biot's coefficient	β	0.9405	
	Damping coefficient	ζ	0	$\mathrm{s^{-1}}$

choose different values for δ in (2.5)–(2.7). In particular, we consider $\delta = 0, \frac{1}{2}, 1$. For the numerical discretization we consider a polygonal decomposition with both quadrilateral and triangular elements of characteristic size $h = 25$, cf. Fig. 6 (right), a polynomial degree $p = r = 3$, a time step $\Delta t = 0.01\ s$ and a final time $T = 1\ s$.

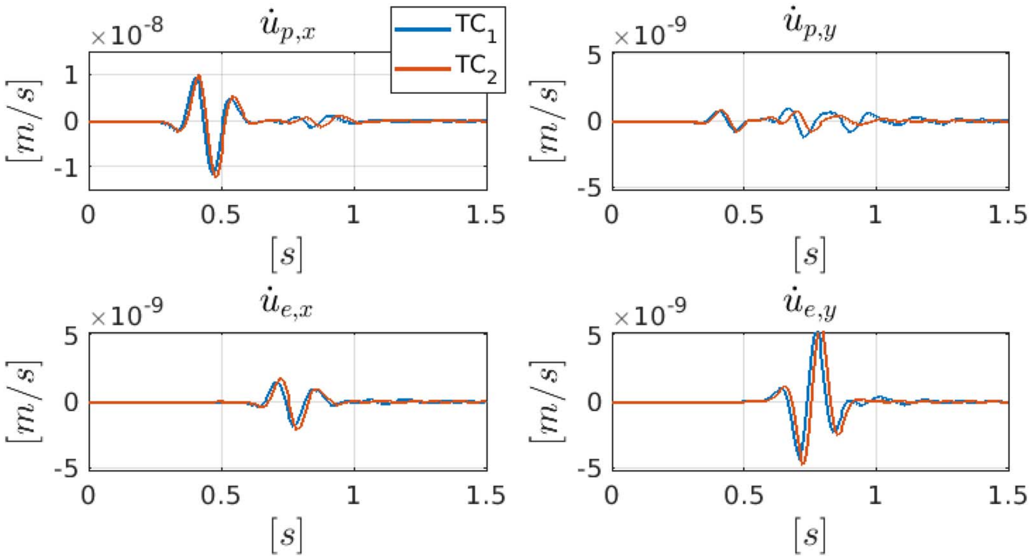

FIG. 8. Test case of Section 6.2. Horizontal and vertical component velocity $\dot{\boldsymbol{u}}_p$ (top) and $\dot{\boldsymbol{u}}_e$ (bottom) for the receivers $\boldsymbol{x}_{r1}$ (top) and $\boldsymbol{x}_{r2}$ (bottom), respectively.

In Fig. 9 we report the snapshots at different times of the computed vertical velocity, for different values of δ. From the results reported in Fig. 9 we see that when the seismic waves, generated by the seismic source, reach the oil and gas reservoirs they are reflected and transmitted. The seismic waves are clearly shown, and we can claim that there is no significant numerical dispersion. We can see the absorbing boundary conditions perform rather well for this complex model, and the seismic waves are absorbed by the boundary elements. The effect of δ is also visible: the more the δ is close to zero, the more the waves remain trapped inside the gas reservoirs. This is in agreement with the model hypothesis in Section 2 (see also Antonietti *et al.* (2022b)).

7. Conclusions

In this work we have presented a space–time PolydG methods for wave propagation problems in coupled poroelastic–elastic media. Based on a displacement weak formulation of the problem we proved stability and error bound for the semidiscretization, where (an interior penalty type) PolydGdG method is considered. Time integration is achieved by an unconditionally stable and implicit dG scheme, which also guarantees high-order accuracy in the time domain. Numerical experiments have been designed, not only to verify the numerical performance of the space–time PolydG method, but also to exploit the flexibility in the process of mesh design offered by polytopic elements. In this respect numerical tests of geophysical interest have been also discussed. The presented space–time PolydG method allows a robust and flexible numerical discretization that can be successfully applied to multiphysics wave propagation problems. Future developments in this direction include the extension to realistic three-dimensional problems, the coupling of this model to fluid-structure (with poroelastic, thermo-elastic or acoustic structure) interaction problems and the design of efficient

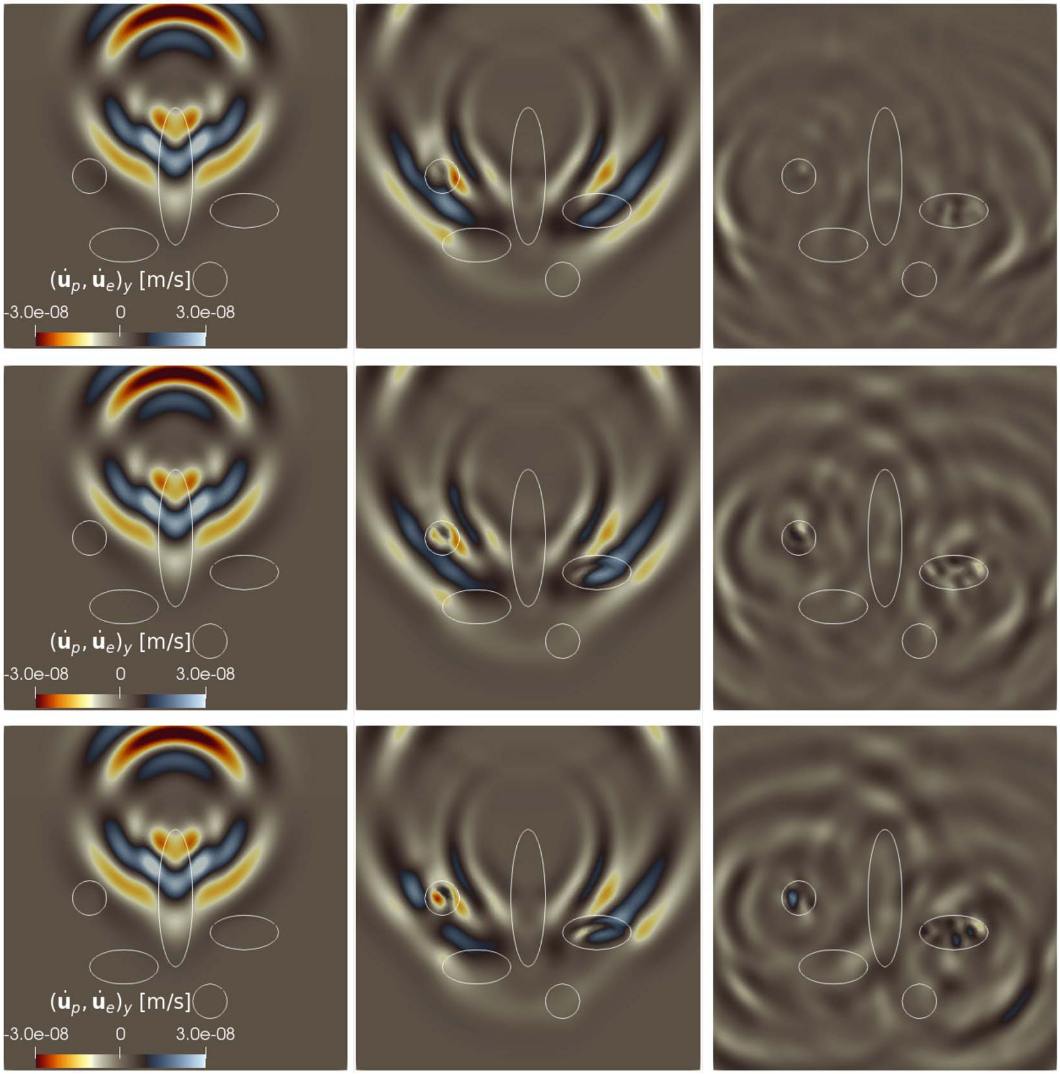

FIG. 9. Test case of Section 6.3. Snapshots of the vertical component velocity $(\dot{\boldsymbol{u}}_p, \dot{\boldsymbol{u}}_e)_y$ at different time instants: from left to right $t = 0.3, 0.4, 0.7$ s; top row $\delta = 1$, middle row $\delta = 0.5$, bottom row $\delta = 0$.

solvers for the solution of the (linear) system of equations stemming from this space–time PolydG discretization.

Acknowledgements

We thank the anonymous reviewers for their valuable insights and comments that greatly contributed to improving the content of this work. This research has been partially funded by the European Union (ERC, NEMESIS, project number 101115663). Views and opinions expressed are however those of the author(s) only and do not necessarily reflect those of the European Union or the European Research Council Executive Agency.

Funding

PRIN2022 grant ASTICE - CUP (D53D23005710006 to I.M.); ICSC-Centro Nazionale di Ricerca in High Performance Computing, Big Data, and Quantu Computing funded by European Union–NextGenerationEU (to P.F.A and I.M.); INdAM-GNCS project CUP E55F22000270001 (to M.B.).

References

Abedi, R., Petracovici, B. & Haber, R. B. (2006) A space–time discontinuous Galerkin method for linearized elastodynamics with element-wise momentum balance. *Comput. Methods Appl. Mech. Eng.*, **195**, 3247–3273.

Agut, C. & Diaz, J. (2013) Stability analysis of the interior penalty discontinuous Galerkin method for the wave equation. *ESAIM Math. Model. Numer. Anal.*, **47**, 903–932.

Ambartsumyan, I., Khattatov, E., Yotov, I. & Zunino, P. (2018) A Lagrange multiplier method for a stokes–Biot fluid–poroelastic structure interaction model. *Numer. Math.*, **140**, 513–553.

Anaya, V., de Wijn, Z., Gómez-Vargas, B., Mora, D. & Ruiz-Baier, R. (2020) Rotation-based mixed formulations for an elasticity-poroelasticity interface problem. *SIAM J. Sci. Comput.*, **42**, B225–B249.

Antonietti, P. F., Bonaldi, F. & Mazzieri, I. (2020a) A high-order discontinuous Galerkin approach to the elasto-acoustic problem. *Comput. Methods Appl. Mech. Eng.*, **358**, 112634.

Antonietti, P. F., Bonaldi, F. & Mazzieri, I. (2020b) Simulation of three-dimensional elastoacoustic wave propagation based on a discontinuous Galerkin spectral element method. *Int. J. Numer. Methods Eng.*, **121**, 2206–2226.

Antonietti, P. F., Bonetti, S. & Botti, M. (2023a) Discontinuous Galerkin approximation of the fully coupled thermo-poroelastic problem. *SIAM J. Sci. Comput.*, **45**, A621–A645.

Antonietti, P. F., Mazzieri, I. & Migliorini, F. (2023b) A discontinuous Galerkin time integration scheme for second order differential equations with applications to seismic wave propagation problems. *Comput. Math. Appl.*, **134**, 87–100.

Antonietti, P. F., Botti, M. & Mazzieri, I. (2022a) On mathematical and numerical modelling of multiphysics wave propagation with polytopal discontinuous Galerkin methods: A review. *Vietnam J. Math.*, **50**, 997–1028.

Antonietti, P. F., Botti, M., Mazzieri, I. & Poltri, S. N. (2022b) A high-order discontinuous Galerkin method for the poro-elasto-acoustic problem on polygonal and polyhedral grids. *SIAM J. Sci. Comput.*, **44**, B1–B28.

Antonietti, P. F., Mazzieri, I., Muhr, M., Nikolić, V. & Wohlmuth, B. (2020c) A high-order discontinuous Galerkin method for nonlinear sound waves. *J. Comput. Phys.*, **415**, 109484.

Antonietti, P. F., Brezzi, F. & Marini, L. D. (2009) Bubble stabilization of discontinuous Galerkin methods. *Comput. Methods Appl. Mech. Eng.*, **198**, 1651–1659.

Antonietti, P. F., Dal Santo, N., Mazzieri, I. & Quarteroni, A. (2018) A high-order discontinuous Galerkin approximation to ordinary differential equations with applications to elastodynamics. *IMA J. Numer. Anal.*, **38**, 1709–1734.

Antonietti, P. F., Giani, S. & Houston, P. (2013) *Hp*-version composite discontinuous Galerkin methods for elliptic problems on complicated domains. *SIAM J. Sci. Comput.*, **35**, A1417–A1439.

Antonietti, P. F. & Mazzieri, I. (2018) High-order discontinuous Galerkin methods for the elastodynamics equation on polygonal and polyhedral meshes. *Comput. Methods Appl. Mech. Eng.*, **342**, 414–437.

Arnold, D. N., Brezzi, F., Cockburn, B. & Marini, L. D. (2001) Unified analysis of discontinuous Galerkin methods for elliptic problems. *SIAM J. Numer. Anal.*, **39**, 1749–1779.

Banks, H. T., Birch, M. J., Brewin, M. P., Greenwald, S. E., Hu, S., Kenz, Z. R., Kruse, C., Maischak, M., Shaw, S. & Whiteman, J. R. (2014) High-order space-time finite element schemes for acoustic and viscodynamic wave equations with temporal decoupling. *Int. J. Numer. Methods Eng.*, **98**, 131–156.

Barucq, H., Calandra, H., Diaz, J. & Shishenina, E. (2018) Space–time Trefftz-dg approximation for elasto-acoustics. *Appl. Anal.*, **99**, 747–760.

Bassi, F., Botti, L., Colombo, A., Di Pietro, D. A. & Tesini, P. (2012) On the flexibility of agglomeration based physical space discontinuous Galerkin discretizations. *J. Comput. Phys.*, **231**, 45–65.

Bause, M., Radu, F. A. & Köcher, U. (2017) Space–time finite element approximation of the Biot poroelasticity system with iterative coupling. *Comput. Methods Appl. Mech. Eng.*, **320**, 745–768.

Bermùdez, A., Rodrìguez, R. & Santamarina, D. (2003) Finite element approximation of a displacement formulation for time-domain elastoacoustic vibrations. *J. Comput. Appl. Math.*, **152**, 17–34.

Biot, M. A. (1955) Theory of elasticity and consolidation for a porous anisotropic solid. *J. Appl. Phys.*, **26**, 182–185.

Bonetti, S., Botti, M., Mazzieri, I. & Antonietti, P. F. (2023) Numerical modeling of wave propagation phenomena in thermo-poroelastic media via discontinuous Galerkin methods. *J. Comput. Phys.*, **489**, 112275.

Bürger, R., Kumar, S., Mora, D., Ruiz-Baier, R. & Verma, N. (2021) Virtual element methods for the three-field formulation of time-dependent linear poroelasticity. *Adv. Comput. Math.*, **47**, 1–37.

Cangiani, A., Dong, Z. & Georgoulis, E. (2022) Hp-version discontinuous Galerkin methods on essentially arbitrarily-shaped elements. *Math. Comp.*, **91**, 1–35.

Cangiani, A., Dong, Z. & Georgoulis, E. H. (2017a) *Hp*-version space-time discontinuous Galerkin methods for parabolic problems on prismatic meshes. *SIAM J. Sci. Comput.*, **39**, A1251–A1279.

Cangiani, A., Dong, Z., Georgoulis, E. H. & Houston, P. (2017b) *Hp-Version Discontinuous Galerkin Methods on Polytopic Meshes* SpringerBriefs in Mathematics. Switzerland: Springer International Publishing.

Cangiani, A., Dong, Z., Georgoulis, E. H. & Houston, P. (2016) *Hp*-version discontinuous Galerkin methods for advection-diffusion-reaction problems on polytopic meshes. *ESAIM Math. Model. Numer. Anal.*, **50**, 699–725.

Cangiani, A., Georgoulis, E. H. & Houston, P. (2014) Hp-version discontinuous Galerkin methods on polygonal and polyhedral meshes. *Math. Models Methods Appl. Sci.*, **24**, 2009–2041.

Carcione, J. (2014) *Wave Fields in Real Media*, vol. **38**. The Netherlands: Elsevier Science.

Castagnede, B., Aknine, A., Melon, M. & Depollier, C. (1998) Ultrasonic characterization of the anisotropic behavior of air-saturated porous materials. *Ultrasonics*, **36**, 323–341.

Chiavassa, G. & Lombard, B. (2013) Wave propagation across acoustic/Biot's media: A finite-difference method. *Commun. Comput. Phys.*, **13**, 985–1012.

Congreve, S. & Houston, P. (2019) Two-grid hp-DGFEMs on agglomerated coarse meshes. *PAMM*, **19**, e201900175.

Dai, N., Vafidis, A. & Kanasewich, E. (1995) Wave propagation in heterogeneous, porous media; a velocity-stress, finite-difference method. *Geophysics*, **60**, 327–340.

De La Puente, J., Dumbser, M., Käser, M. & Igel, H. (2008) Discontinuous Galerkin methods for wave propagation in poroelastic media. *Geophysics*, **73**, T77–T97.

Delfour, M., Hager, W. & Trochu, F. (1981) Discontinuous Galerkin methods for ordinary differential equations. *Math. Comp.*, **36**, 455–473.

Dörfler, W., Findeisen, S. & Wieners, C. (2016) Space-time discontinuous Galerkin discretizations for linear first-order hyperbolic evolution systems. *Comput. Methods Appl. Math.*, **16**, 409–428.

Dupuy, B., De Barros, L., Garambois, S. & Virieux, J. (2011) Wave propagation in heterogeneous porous media formulated in the frequency-space domain using a discontinuous Galerkin method. *Geophysics*, **76**, N13–N28.

Ezziani, A. (2005) *Modélisation mathématique et numérique de la Propagation d'ondes Dans les Milieux viscoélastiques et poroélastiques* Theses. ENSTA ParisTech.

Ferro, M. & Mansur, W. (2006) Wave propagation in elastic and poroelastic media in the frequency domain by the boundary element method. *28th World conference on boundary elements and other mesh reduction methods. WIT transactions on modelling and simulation* (C. A. Brebbia & J. T. Katsikadelis eds), vol. **42**. Southampton, UK: WIT Press, pp. 285–293.

Flemisch, B., Kaltenbacher, M., Triebenbacher, S. & Wohlmuth, B. (2010) The equivalence of standard and mixed finite element methods in applications to elasto-acoustic interaction. *SIAM J. Sci. Comput.*, **32**, 1980–2006.

Flemisch, B., Kaltenbacher, M. & Wohlmuth, B. (2006) Elasto-acoustic and acoustic-acoustic coupling on non-matching grids. *Int. J. Numer. Methods Eng.*, **67**, 1791–1810.

French, D. A. (1993) A space-time finite element method for the wave equation. *Comput. Methods Appl. Mech. Eng.*, **107**, 145–157.

Girault, V., Pencheva, G., Wheeler, M. & Wildey, T. (2011) Domain decomposition for poroelasticity and elasticity with dg jumps and mortars. *Math. Models Methods Appl. Sci.*, **21**, 169–213.

Gopalakrishnan, J., Schöberl, J. & Wintersteiger, C. (2017) Mapped tent pitching schemes for hyperbolic systems. *Comput. Methods Sci. Eng.*, **39**, B1043–B1063.

Gregor, D., Moczo, P., Kristek, J., Mesgouez, A., Lefeuve-Mesgouez, G., Morency, C., Diaz, J. & Kristekova, M. (2021) Seismic waves in medium with poroelastic/elastic interfaces: A two-dimensional P-SV finite-difference modelling. *Geophys. J. Int.*, **228**, 551–588.

Haire, T. & Langton, C. (1999) Biott theory: A review of its application to ultrasound propagation through cancellous bone. *Bone*, **24**, 291–295.

He, Y., Chen, T. & Gao, J. (2019) Unsplit perfectly matched layer absorbing boundary conditions for second-order poroelastic wave equations. *Wave Motion*, **89**, 116–130.

Hughes, T. & Hulbert, G. (1988) Space-time finite element methods for elastodynamics: Formulation and error estimates. *Comput. Methods Appl. Mech. Eng.*, **66**, 339–363.

Jay, L. O. (2015) *Lobatto Methods*. Berlin, Heidelberg: Springer Berlin Heidelberg, pp. 817–826.

Johnson, C. (1993) Discontinuous Galerkin finite element methods for second order hyperbolic problems. *Comput. Methods Appl. Mech. Eng.*, **107**, 117–129.

Kretzschmar, F., Moiola, A., Perugia, I. & Schenpp, S. M. (2016) *A priori* error analysis of space-time Trefftz discontinuous Galerkin methods for wave problems. *IMA J. Numer. Anal.*, **36**, 1599–1635.

Krishnan, B., Raja, D. M. S. & Venkataramana, K. (2015) Structural and Vibroacoustic analysis of aircraft fuselage section with passive noise reducing materials: A material performance study. *4th International Engineering Symposium*. London: Elsevier.

Lefeuve-Mesgouez, G., Mesgouez, A., Chiavassa, G. & Lombard, B. (2012) Semi-analytical and numerical methods for computing transient waves in 2d acoustic/poroelastic stratified media. *Wave Motion*, **49**, 667–680.

Martin, R., Komatitsch, D. & Ezziani, A. (2008) An unsplit convolutional perfectly matched layer improved at grazing incidence for seismic wave propagation in poroelastic media. *Geophysics*, **73**, T51–T61.

Masson, Y. J. & Pride, S. R. (2010) Finite-difference modeling of Biot's poroelastic equations across all frequencies. *Geophysics*, **75**, N33–N41.

Moiola, A. & Perugia, I. (2018) A space–time Trefftz discontinuous Galerkin method for the acoustic wave equation in first-order formulation. *Numer. Math.*, **138**, 389–435.

Morency, C., Luo, Y. & Tromp, J. (2011) Acoustic, elastic and poroelastic simulations of CO2 sequestration crosswell monitoring based on spectral-element and adjoint methods. *Geophys. J. Int.*, **185**, 955–966.

Morency, C. & Tromp, J. (2008) Spectral-element simulations of wave propagation in porous media. *Geophys. J. Int.*, **175**, 301–345.

Nochetto, R. H., Sauter, S. A. & Wieners, C. (2018) Space-time methods for time-dependent partial differential equations. *Oberwolfach Reports*, **14**, 863–947.

Peng, H., Sripanich, Y., Vasconcelos, I. & Trampert, J. (2021) Benchmarking wave equation solvers using interface conditions: The case of porous media. *Geophys. J. Int.*, **224**, 355–376.

Perugia, I., Schöberl, J., Stocker, P. & Wintersteiger, C. (2020) Tent pitching and Trefftz-dg method for the acoustic wave equation. *Comput. Math. Appl.*, **79**, 2987–3000.

Phillips, P. J. & Wheeler, M. F. (2008) A coupling of mixed and discontinuous Galerkin finite-element methods for poroelasticity. *Comput. Geosci.*, **12**, 417–435.

Quarteroni, A., Sacco, R. & Saleri, F. (2007) *Numerical Mathematics*, vol. **37**. Berlin, Heidelberg: Springer.

Rockafellar, R. T. (1993) Lagrange multipliers and optimality. *SIAM Rev.*, **35**, 183–238.

Schötzau, D. & Schwab, C. (2000) Time discretization of parabolic problems by the *hp*-version of the discontinuous Galerkin finite element method. *SIAM J. Numer. Anal.*, **38**, 837–875.

Sidler, R., Carcione, J. M. & Holliger, K. (2010) Simulation of surface waves in porous media. *Geophys. J. Int.*, **183**, 820–832.

Southworth, B. S., Krzysik, O., Pazner, W. & Sterck, H. D. (2022) Fast solution of fully implicit Runge–Kutta and discontinuous Galerkin in time for numerical PDEs, part I: The linear setting. *SIAM J. Sci. Comput.*, **44**, A416–A443.

Souzanchi, M., Cardoso, L. & Cowin, S. (2013) Tortuosity and the averaging of microvelocity fields in poroelasticity. *J. Appl. Mech.*, **80**, 0209061–0209065.

Stacey, R. (1988) Improved transparent boundary formulations for the elastic-wave equation. *Bull. Seismol. Soc. Am.*, **78**, 2089–2097.

Stein, E. M. (1970) *Singular Integrals and Differentiability Properties of Functions*, vol. **2**. Princeton, New Jersey, US: Princeton University Press.

Triebenbacher, S., Kaltenbacher, M., Wohlmuth, B. & Flemisch, B. (2010) Applications of the mortar finite element method in vibroacoustics and flow induced noise computations. *Acta Acust. United Acust.*, **96**, 536–553(18).

Van Der Vegt, J., Klaji, C., Van Der Bos, F. & Van Der Ven, H. (2006) Space-time discontinuous Galerkin method for the compressible Navier-stokes equations on deforming meshes. *European Conference on Computational Fluid Dynamics ECCOMAS CFD*, **2006**, 1–11.

Vashisth, A. K., Sharma, M. D. & Gogna, M. L. (1991) Reflection and transmission of elastic waves at a loosely bonded interface between an elastic solid and liquid-saturated porous solid. *Geophys. J. Int.*, **105**, 601–617.

Ward, N. D., Lähivaara, T. & Eveson, S. (2017) A discontinuous Galerkin method for poroelastic wave propagation: The two-dimensional case. *J. Comput. Phys.*, **350**, 690–727.

Wenzlau, F. & Müller, T. M. (2009) Finite-difference modeling of wave propagation and diffusion in poroelastic media. *Geophysics*, **74**, T55–T66.

Zhan, Q., Zhuang, M., Mao, Y. & Liu, Q. H. (2020) Unified Riemann solution for multi-physics coupling: Anisotropic poroelastic/elastic/fluid interfaces. *J. Comput. Phys.*, **402**, 108961.

Zhang, Y. & Gao, J. (2014) A 3d staggered-grid finite difference scheme for poroelastic wave equation. *J. Appl. Geophys.*, **109**, 281–291.

Zhang, Y., Gao, J., Han, W. & He, Y. (2019) A discontinuous Galerkin method for seismic wave propagation in coupled elastic and poroelastic media. *Geophys. Prospect.*, **67**, 1392–1403.

Appendix A. Definition of the coupling bilinear form

The aim of this appendix is to motivate the definition of $\mathcal{C}_h(\cdot,\cdot)$ adopted in Section 3.1. We consider equations (2.1) and (2.3), and we multiply them by test functions $\boldsymbol{w}_e \in \mathbf{V}_\mathbf{h}^\mathbf{e}$ and $\boldsymbol{w}_p, \boldsymbol{w}_f \in \mathbf{V}_\mathbf{h}^\mathbf{p}$, respectively, integrate by parts element-wise and focus only to the interface terms, i.e., integrals on Γ_I, namely,

$$\begin{aligned}\sum_{i=1}^{5} T_i = &- \int_{\Gamma_I} \boldsymbol{\sigma}_e(\boldsymbol{u}_e)\boldsymbol{n}_e \cdot \boldsymbol{w}_e \,\mathrm{d}s - \int_{\Gamma_I} \boldsymbol{\sigma}_e(\boldsymbol{u}_p)\boldsymbol{n}_p \cdot \boldsymbol{w}_p \,\mathrm{d}s \\ &+ \delta \int_{\Gamma_I} \beta p(\boldsymbol{u}_p, \boldsymbol{u}_f)\boldsymbol{w}_p \cdot \boldsymbol{n}_p \,\mathrm{d}s + (1-\delta)\int_{\Gamma_I} \beta p(\boldsymbol{u}_p, \boldsymbol{u}_f)\boldsymbol{w}_p \cdot \boldsymbol{n}_p \,\mathrm{d}s \\ &+ \int_{\Gamma_I} p(\boldsymbol{u}_p, \boldsymbol{u}_f)\boldsymbol{w}_f \cdot \boldsymbol{n}_p \,\mathrm{d}s,\end{aligned}$$

removing the subscript h to ease the notation. Next, we notice that, in view of condition (2.5), the terms $T_1 + T_2 + T_3$ can be rewritten as

$$T_1 + T_2 + T_3 = -\int_{\Gamma_I} \boldsymbol{\sigma}_e(\boldsymbol{u}_e)\boldsymbol{n}_p \cdot (\boldsymbol{w}_p - \boldsymbol{w}_e)\,\mathrm{d}s, \tag{A.1}$$

while $T_4 + T_5$ as

$$T_4 + T_5 = -\int_{\Gamma_I} m\nabla \cdot (\beta \boldsymbol{u}_p + \boldsymbol{u}_f)((1-\delta)\beta \boldsymbol{w}_p + \boldsymbol{w}_f) \cdot \boldsymbol{n}_p \,\mathrm{d}s. \tag{A.2}$$

Then, we add to (A.1) and (A.2) the following strongly consistent terms to ensure the symmetry and positivity of the resulting system:

$$-\int_{\Gamma_I} \boldsymbol{\sigma}_e(\boldsymbol{v}_e)\boldsymbol{n}_p \cdot (\boldsymbol{u}_p - \boldsymbol{u}_e)\,\mathrm{d}s + \int_{\Gamma_I} \alpha(\boldsymbol{u}_p - \boldsymbol{u}_e) \cdot (\boldsymbol{v}_p - \boldsymbol{v}_e)\,\mathrm{d}s, \tag{A.3}$$

and

$$\begin{aligned} &-\int_{\Gamma_I} m\nabla \cdot (\beta \boldsymbol{w}_p + \boldsymbol{w}_f)((1-\delta)\beta \boldsymbol{u}_p + \boldsymbol{u}_f) \cdot \boldsymbol{n}_p \,\mathrm{d}s \\ &\qquad + \gamma \int_{\Gamma_I} ((1-\delta)\beta \boldsymbol{u}_p + \boldsymbol{u}_f) \cdot \boldsymbol{n}_p((1-\delta)\beta \boldsymbol{v}_p + \boldsymbol{v}_f) \cdot \boldsymbol{n}_p \,\mathrm{d}s, \end{aligned} \tag{A.4}$$

with α and γ defined as in (3.5)–(3.6). Finally, summing up equations (A.1)–(A.4) we get

$$\begin{aligned} \mathcal{C}_h(\boldsymbol{U}, \boldsymbol{W}) = &- \langle \boldsymbol{\sigma}_e(\boldsymbol{u}_e)\boldsymbol{n}_p, \boldsymbol{w}_p - \boldsymbol{w}_e\rangle_{\mathcal{F}_h^I} - \langle \boldsymbol{\sigma}_e(\boldsymbol{v}_e)\boldsymbol{n}_p, \boldsymbol{u}_p - \boldsymbol{u}_e\rangle_{\mathcal{F}_h^I} + \langle \alpha \boldsymbol{u}_p - \boldsymbol{u}_e, \boldsymbol{v}_p - \boldsymbol{v}_e\rangle_{\mathcal{F}_h^I} \\ &- \langle m\nabla \cdot (\beta \boldsymbol{u}_p + \boldsymbol{u}_f), ((1-\delta)\beta \boldsymbol{w}_p + \boldsymbol{w}_f) \cdot \boldsymbol{n}_p\rangle_{\Gamma_I} \\ &- \langle m\nabla \cdot (\beta \boldsymbol{w}_p + \boldsymbol{w}_f), ((1-\delta)\beta \boldsymbol{u}_p + \boldsymbol{u}_f) \cdot \boldsymbol{n}_p\rangle_{\mathcal{F}_h^I} \\ &+ \gamma\langle ((1-\delta)\beta \boldsymbol{u}_p + \boldsymbol{u}_f) \cdot \boldsymbol{n}_p, ((1-\delta)\beta \boldsymbol{v}_p + \boldsymbol{v}_f) \cdot \boldsymbol{n}_p\rangle_{\mathcal{F}_h^I}, \end{aligned} \tag{A.5}$$

which is definition (3.7). Note that $\mathcal{C}_h(\boldsymbol{U}, \boldsymbol{W}) = \mathcal{C}_h(\boldsymbol{W}, \boldsymbol{U})$.

Appendix B. Sketch of the proof of Lemma 5.3

We consider the error vector component-wise, i.e., $\boldsymbol{E} = (\boldsymbol{E}^u, \boldsymbol{E}^v) = (\boldsymbol{U} - \boldsymbol{U}_{dG}, \boldsymbol{V} - \boldsymbol{V}_{dG})$, and use similar notation for $\boldsymbol{E}_I$ and $\boldsymbol{E}_h$. We consider (5.7) and choose $\boldsymbol{W} = (\boldsymbol{U}, \boldsymbol{V}) = (B\boldsymbol{E}_h^v, M^{-1}B\boldsymbol{E}_h^u)$, where $B = A + C$ to obtain

$$\mathcal{A}_{\mathrm{T}}((\boldsymbol{E}_h^u, \boldsymbol{E}_h^v), (B\boldsymbol{E}_h^v, M^{-1}B\boldsymbol{E}_h^u)) = -\mathcal{A}_{\mathrm{T}}((\boldsymbol{E}_I^u, \boldsymbol{E}_I^v), (B\boldsymbol{E}_h^v, M^{-1}B\boldsymbol{E}_h^u)),$$

which we can rewrite as

$$
\begin{aligned}
&\sum_{n=1}^{N}(\dot{\boldsymbol{E}}_h^u, B\boldsymbol{E}_h^v)_{I_n} - \sum_{n=1}^{N}(\boldsymbol{E}_h^v, B\boldsymbol{E}_h^v)_{I_n} + \sum_{n=0}^{N-1}[\boldsymbol{E}_h^u]_n \cdot B\boldsymbol{E}_h^v(t_n^+) + \sum_{n=1}^{N}(\dot{\boldsymbol{E}}_h^v, B\boldsymbol{E}_h^u)_{I_n} \\
&\qquad + \sum_{n=1}^{N}(M^{-1}D\boldsymbol{E}_h^v, B\boldsymbol{E}_h^u)_{I_n} + \sum_{n=1}^{N}(M^{-1}B\boldsymbol{E}_h^u, B\boldsymbol{E}_h^u)_{I_n} + \sum_{n=0}^{N-1}[\boldsymbol{E}_h^v]_n \cdot B\boldsymbol{E}_h^u(t_n^+) \\
&= \sum_{n=1}^{N} -(\dot{\boldsymbol{E}}_I^u, B\boldsymbol{E}_h^v)_{I_n} + \sum_{n=1}^{N}(\boldsymbol{E}_I^v, B\boldsymbol{E}_h^v)_{I_n} - \sum_{n=0}^{N-1}[\boldsymbol{E}_I^u]_n \cdot B\boldsymbol{E}_h^v(t_n^+) - \sum_{n=1}^{N}(\dot{\boldsymbol{E}}_I^v, B\boldsymbol{E}_h^u)_{I_n} \\
&\qquad - \sum_{n=1}^{N}(M^{-1}D\boldsymbol{E}_I^v, B\boldsymbol{E}_h^u)_{I_n} - \sum_{n=1}^{N}(M^{-1}B\boldsymbol{E}_I^u, B\boldsymbol{E}_h^u)_{I_n} - \sum_{n=0}^{N-1}[\boldsymbol{E}_I^v]_n \cdot B\boldsymbol{E}_h^u(t_n^+),
\end{aligned}
\tag{B.1}
$$

where we have implicitly used that $\boldsymbol{E}_h^u(0^-) = \boldsymbol{E}_h^v(0^-) = \boldsymbol{E}_I^u(0^-) = \boldsymbol{E}_I^v(0^-) = \boldsymbol{0}$. Next, integrating the first term on the left-hand side and the first term on the right-hand side of (B.1), and using the properties of the projection operator in (5.8), we can obtain

$$
\begin{aligned}
&\sum_{n=1}^{N}(M^{-1}B\boldsymbol{E}_h^u, B\boldsymbol{E}_h^u)_{I_n} + \sum_{n=1}^{N}(M^{-1}D\boldsymbol{E}_h^v, B\boldsymbol{E}_h^u)_{I_n} - \sum_{n=1}^{N}(\boldsymbol{E}_h^v, B\boldsymbol{E}_h^v)_{I_n} + \sum_{n=0}^{N-1}B[\boldsymbol{E}_h^u]_n \cdot \boldsymbol{E}_h^v(t_n^+) \\
&\qquad + \sum_{n=0}^{N-1}\left(B\boldsymbol{E}_h^u(t_{n+1}^-) \cdot \boldsymbol{E}_h^v(t_{n+1}^-) - B\boldsymbol{E}_h^u(t_n^+) \cdot \boldsymbol{E}_h^v(t_n^+)\right) + \sum_{n=0}^{N-1}B[\boldsymbol{E}_h^v]_n \cdot \boldsymbol{E}_h^u(t_n^+) \\
&= \sum_{n=1}^{N}(\boldsymbol{E}_\pi^v, B\boldsymbol{E}_h^v)_{I_n} - (M^{-1}D\boldsymbol{E}_I^v, B\boldsymbol{E}_h^u)_{I_n} + (M^{-1}B\boldsymbol{E}_I^u, B\boldsymbol{E}_h^u)_{I_n},
\end{aligned}
\tag{B.2}
$$

where we also used that B is symmetric. Then, a simple manipulation leads to

$$
\begin{aligned}
\sum_{n=1}^{N}(M^{-1}B\boldsymbol{E}_h^u, B\boldsymbol{E}_h^u)_{I_n} &= -\sum_{n=1}^{N}(M^{-1}D\boldsymbol{E}_h^v, B\boldsymbol{E}_h^u)_{I_n} + \sum_{n=1}^{N}(\boldsymbol{E}_h^v, B\boldsymbol{E}_h^v)_{I_n} \\
&\quad - B\boldsymbol{E}_h^u(0^+) \cdot \boldsymbol{E}_h^v(0^+) - \sum_{n=0}^{N-1}B[\boldsymbol{E}_h^v]_n \cdot [\boldsymbol{E}_h^u]_n - B\boldsymbol{E}_h^u(T^-) \cdot \boldsymbol{E}_h^v(T^-) \\
&\quad + \sum_{n=1}^{N}(\boldsymbol{E}_I^v, B\boldsymbol{E}_h^v)_{I_n} - (M^{-1}D\boldsymbol{E}_I^v, B\boldsymbol{E}_h^u)_{I_n} + (M^{-1}B\boldsymbol{E}_I^u, B\boldsymbol{E}_h^u)_{I_n}.
\end{aligned}
$$

Finally, we use Cauchy–Schwarz and Young inequalities to have

$$\begin{aligned}
\sum_{n=1}^{N} \|B\boldsymbol{E}_h^u\|_{0,I_n}^2 \lesssim & \sum_{n=1}^{N} \frac{1}{2\varepsilon_1} \|\boldsymbol{E}_h^v\|_{0,I_n}^2 + \frac{\varepsilon_1}{2} \|B\boldsymbol{E}_h^u\|_{0,I_n}^2 + \sum_{n=1}^{N} \|\boldsymbol{E}_h^v\|_{0,I_n}^2 \\
& + \frac{1}{2}(B^{\frac{1}{2}}\boldsymbol{E}_h^u(0^+))^2 + \frac{1}{2}\sum_{n=0}^{N-1}(B^{\frac{1}{2}}[\boldsymbol{E}_h^v]_n)^{\frac{1}{2}} + \frac{1}{2}(B^{\frac{1}{2}}\boldsymbol{E}_h^u(T^-))^{\frac{1}{2}} \\
& + \frac{1}{2}(B^{\frac{1}{2}}\boldsymbol{E}_h^u(0^+))^2 + \frac{1}{2}\sum_{n=0}^{N-1}(B^{\frac{1}{2}}[\boldsymbol{E}_h^v]_n)^{\frac{1}{2}} + \frac{1}{2}(B^{\frac{1}{2}}\boldsymbol{E}_h^u(T^-))^{\frac{1}{2}} \\
& + \sum_{n=1}^{N} \frac{1}{2}\|\boldsymbol{E}_I^v\|_{0,I_n}^2 + \frac{1}{2}\|\boldsymbol{E}_h^v\|_{0,I_n}^2 + \sum_{n=1}^{N} \frac{1}{2\varepsilon_2}\|\boldsymbol{E}_I^v\|_{0,I_n}^2 + \frac{\varepsilon_2}{2}\|B\boldsymbol{E}_h^u\|_{0,I_n}^2 \\
& + \sum_{n=1}^{N} \frac{1}{2\varepsilon_3}\|\boldsymbol{E}_I^u\|_{0,I_n}^2 + \frac{\varepsilon_3}{2}\|B\boldsymbol{E}_h^u\|_{0,I_n}^2,
\end{aligned}$$

for any positive $\varepsilon_1, \varepsilon_2$ and ε_3. Now, choosing $\varepsilon_1, \varepsilon_2$ and ε_3 small enough we obtain

$$\sum_{n=1}^{N} \|B\boldsymbol{E}_h^u\|_{0,I_n}^2 \lesssim |\boldsymbol{E}_h|_{dG}^2 + \sum_{n=1}^{N} \|\boldsymbol{E}_I^v\|_{0,I_n}^2 + \|\boldsymbol{E}_I^u\|_{0,I_n}^2.$$

Finally, we obtain the proof by observing that

$$\sum_{n=1}^{N} \|\widehat{A}\boldsymbol{E}_h\|_{0,I_n}^2 = \sum_{n=1}^{N} \|B\boldsymbol{E}_h^u\|_{0,I_n}^2 + \|\boldsymbol{E}_h^v\|_{0,I_n}^2.$$